2.06 Thermal Properties of Irradiated UO_2 and MOX☆

Dragos Staicu, European Commission, Joint Research Centre, Karlsruhe, Germany

Abbreviations

DPA displacements per atom
EOL end of life
ERV elementary representative volume
FP fission product
HBRP high burnup rim project
HBS high burnup structure
LWR light water reactor
MOX mixed oxide $(U,Pu)O_2$
NFI nuclear fuel industries
NFIR nuclear fuel industry research
PNNL Pacific Northwest National Laboratory
SIMFUEL simulated high burnup fuel
TD theoretical density

Symbols

Bu Burnup (MWd kg HM^{-1})
C_p Specific heat (J g^{-1} K^{-1})
T Temperature (K)
T_{ann} Annealing temperature (K)
T_c Temperature (°C)

☆*Change History*: July 2019. Dragos Staicu updated the article by adding a section on the melting point and updated reference list.
This is an update of Staicu, D., 2012. Chapter 2.17 – Thermal Properties of Irradiated UO_2 and MOX. In: Konings, R.J.M. (Ed.), Comprehensive Nuclear Materials, Elsevier, pp. 439–464.

T_{irr} Irradiation temperature (K)
T_M Melting temperature (K)
x Deviation from stoichiometry
λ Thermal conductivity (W m^{-1} K^{-1})
λ_{95} Thermal conductivity normalized to 5 vol% porosity (W m^{-1} K^{-1})
ρ Density (kg m^{-3})

2.06.1 Introduction: Importance of Thermal Conductivity and Melting Temperature

Knowledge of the thermal conductivity of the fuel of a nuclear reactor is required for the prediction of fuel performance during irradiation, in particular for the determination of the temperature distribution and of the fission gas release.

The principal objectives of this article are to give elements useful to understand the phenomena causing the degradation of the thermal conductivity during irradiation and to provide guidance for the interpretation and comparison of in-pile or out-of-pile measurements, especially as a function of burnup and for samples having different irradiation temperatures, in-pile histories, and microstructures. The importance of such studies is more significant when the discharge burnup of the fuel is increased and with the formation of the high burnup structure (HBS), because these two parameters have a significant impact on the thermal conductivity. The impact of the introduction of plutonium or additives (Gd, Cr, etc.) in standard UO_2 also requires assessment. Uranium–plutonium mixed oxide (MOX) fuel represents a significant fraction of the nuclear fuel used in commercial light water reactors (LWRs). The industrial processes used for the production of MOX fuel are based on the mixing of a few percent of plutonium oxide with UO_2. The different microstructures that can be obtained are mainly characterized by the degree of homogeneity of the plutonium distribution. The impact of the introduction of plutonium in UO_2 and the different microstructures therefore need to be considered because the presence of Pu in the UO_2 lattice will reduce the thermal conductivity. UO_2 fuel with increased grains size is produced by doping with chromium oxide, with the objectives of reducing the pellet–cladding interaction by an increased viscoplasticity and of reducing fission gas release. This section mainly deals with LWR fuel because of the lack of data for irradiated fast reactor fuel.

The specific heat of the fuel is also affected by irradiation. This parameter is required for the investigation of fuel performance during transients and also for the calculation of the thermal conductivity from thermal diffusivity measurements. The evolution of the thermal conductivity as a function of burnup is nonlinear, and numerous approaches and approximations are used, leading to a large number of publications on this subject. This is not the case for the specific heat which generally obeys the law of mixtures. The thermal expansion and oxygen potential of the fuel are also important for fuel performance studies, but they are not addressed in this section.

The thermal conductivity distributions as a function of the radial position in a pellet for two temperature profiles (central temperatures of 1000 and 1500K) and for burnups of 0 (fresh fuel) and 40 MWd kg HM^{-1} calculated with the equation of Ronchi *et al.*[1] are shown in Fig. 1. A large temperature gradient exists over the small distance between the pellet center and the pellet rim, inducing large variations in the conductivity. It can be seen that the conductivity decreases with temperature and burnup.

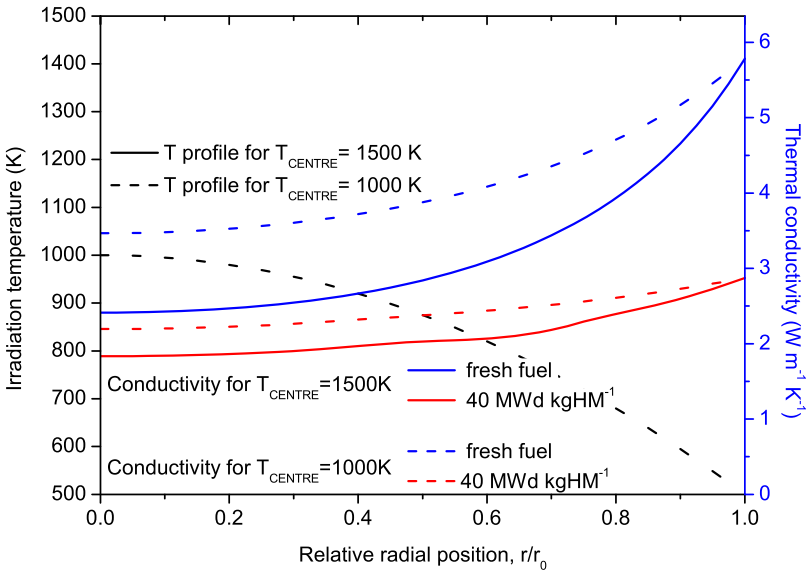

Fig. 1 Thermal conductivity distribution[1] as a function of the radial position in a pellet, for two temperature profiles and for burnups of 0 (fresh fuel) and 40 MWd kg HM^{-1}.

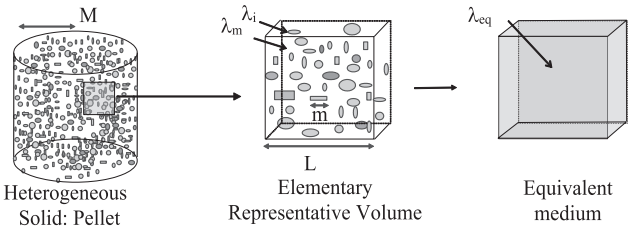

Fig. 2 Notion of separation of scales: an elementary representative volume exists for the heat transfer, with $M \gg L \gg m$.

Under steady-state irradiation conditions and assuming a purely radial heat transfer, the temperature distribution $T(r)$ in a fuel pellet is given by Eq. (1) and depends on the local thermal conductivity $\lambda(r,T)$ and volumetric heat generation rate $q(r)$.

$$\frac{1}{r}\frac{\mathrm{d}}{\mathrm{d}r}\left(r \cdot \lambda(r,T)\frac{\mathrm{d}T(r)}{\mathrm{d}r}\right) + q(r) = 0 \tag{1}$$

The local thermal conductivity $\lambda(r,T)$ depends on the radial position and local temperature. The radial dependence of the thermal conductivity is linked to the local values of the burn-up, porosity, irradiation damage concentration and stoichiometry. The local heat generation rate requires information on the fission cross sections and depends on the radial distribution of the thermal neutron flux and of the fissile isotopes. This distribution changes during irradiation as a result of the consumption of the initial fissile isotopes and the production of fissile Pu.

From the point of view of heat transfer, both fresh and irradiated fuels are heterogeneous materials (e.g., due to the presence of the porosity). However, fresh fuels can be considered as homogeneous, even the heterogeneous MOX, and an effective or equivalent thermal conductivity can be defined. This is because the size of the pores and the plutonium-rich agglomerates is small (compared with the dimensions of the pellet) and has a uniform distribution as required by fuel fabrication specification. The heterogeneity is higher in irradiated fuel because irradiation induces the formation of numerous elements and compounds, bubbles, fission products precipitates, etc., with concentrations depending on the radial position.

The definition of the effective thermal conductivity of a heterogeneous material such as irradiated fuel is not straightforward. The different scales that may be considered for the heat transfer are shown in **Fig. 2**, where m is the microscale corresponding to the size of the larger heterogeneities, L is the mesoscale corresponding to the elementary representative volume (ERV), and M is the macroscale corresponding to the pellet radius. The thermal conductivities of the matrix and of the inclusions are noted λ_m and λ_i, respectively. If the separation of scales is verified,[2] $M \gg L \gg m$ and the equivalent thermal conductivity λ_{eq} is defined from the mean temperature gradient $\langle \nabla T \rangle$ and the mean density of the heat flux $\langle \phi \rangle$ within the ERV: $\lambda_{eq} = -\langle \phi \rangle / \langle \nabla T \rangle$.

The equivalent thermal conductivity λ_{eq} can be evaluated from the conductivity and the geometric distribution of the constituents provided the following criteria are met:

(1) If the equivalent conductivity is evaluated over a volume V, and there exists a value of V beyond which the value of the conductivity no longer varies as V is increased, this volume is the ERV.
(2) The medium is statistically homogeneous: the statistical distribution of the phases does not depend on the position within the material, and the equivalent conductivity is the same irrespective of the position of the ERV.
(3) The dimensions of the material are large compared with the dimensions of the ERV.
(4) Steady-state heat transfer is assumed. For transient heat transfer, homogenization is inappropriate, and the real microstructure has to be considered.
(5) The medium is opaque to thermal radiation.
(6) Fourier's law applies within the ERV and in the entire medium.
(7) No mass transfer is involved.
(8) No internal heat sources exist.

The first three criteria, relating to the microstructure, are not perfectly met for irradiated fuel. A rigorous homogenization is therefore not possible because the thermal conductivity depends on the radial position in the pellet as a result of the radial distribution of burnup and the irradiation temperature. However, a local homogenization is usually made by assuming that over a small radial position interval, the characteristics of the fuel are constant and allow the measurement or calculation of an effective thermal conductivity. For standard irradiated fuels, the unit cell required for homogenization has dimensions of about 1 mm^3, considering that the biggest heterogeneities have a size up to 100 μm, these can be pores or Pu rich agglomerates in heterogeneous MOX fuels. However, burnup and irradiation temperature are not constant over a radial interval of 1 mm, and therefore this unit cell is not rigorously suited for homogenization. Homogenization can be accomplished in a more rigorous way in the case of disk fuels obtained during test irradiations, if almost uniform burnup and irradiation temperature profiles are obtained. This homogenization allows an average temperature field to be calculated, and the corresponding equivalent thermal conductivity will be used to calculate the macroscopic radial temperature gradient in the fuel. Local temperature variations exist, for instance, because of plutonium-rich zones or a particular local arrangement or shape of the pores or cracks.

The criteria 4–6 are met for irradiated fuel. The seventh criterion can be considered as met because the effect of mass transfer is negligible for LWR fuels: some elements migrate as a result of the gradients in the pellet, but the heat transferred by this mechanism is small when compared to conduction. The eighth criterion is not met when the effective thermal conductivity is deduced from in-pile temperature measurements. The intensity of the internal heat sources (for instance in the Pu rich agglomerates of the heterogeneous MOX) should not be considered when the effective thermal conductivity of heterogeneous fuels is evaluated, for instance, from finite-element temperature calculations. The reason is that if the heat sources would be switched on during the effective conductivity calculation, the determined effective thermal conductivity would depend on their intensity.

The thermal properties of irradiated fuels are investigated in pile by temperature measurements and out of pile by thermal diffusivity measurements. Theoretical studies exist for the effect of some single parameters. Direct out-of-pile measurements on irradiated fuel samples appear more reliable because of the well-defined and optimized measurement parameters, although the in-pile conditions cannot be completely reproduced (temperature gradient, fission rate, etc.). Therefore, in-pile determinations are indispensable, even though the deduction of the thermal conductivity from Eq. (1) is less accurate because other parameters like the gap conductance need to be calculated. The published correlations range from empirical formulae to more sophisticated models integrating explicitly and semiempirically the effect of some parameters. A new correlation is often a combination of different existing approaches, for instance, fresh fuels results, out-of-pile experiments on simulated or real irradiated samples, and correlations obtained from in-pile temperature measurements.

No consensus exists on the most reliable correlation and usually, fuel performance codes incorporate a number of correlations, leaving it to the user to select which is the most appropriate for a specific case. For instance, the FEMAXI-6 code[3] includes about 10 thermal conductivity correlations for irradiated UO_2. Before presenting the most representative results, the different burnup effects that have an impact on the thermal conductivity are discussed individually.

The effect of burn-up on the melting temperature needs to be known for the determination of the fuel behavior under transient or accidental conditions and for the definition of the margin to melt. This property is reviewed in the last section of this article.

2.06.2 Parameters Determining the Thermal Conductivity

The composition, atomic structure, and microstructure of an irradiated fuel are complex and evolve during irradiation. Because the thermal conductivity depends on each of these characteristics, a large number of parameters are required to determine its value. At the mesoscopic scale, the main relevant parameters are the microstructure (porosity, grains size, fission gas bubbles, and plutonium or additives distribution) and the precipitates. The parameters acting at the microscopic (atomic) scale are plutonium and the additives that are dissolved in the lattice, the soluble and insoluble fission products and fission gases dispersed as atoms, radiation damage (interstitials, vacancies), bubbles, dislocations, stoichiometry. It should be kept in mind that the thermal conductivity is impacted by the fission density: the instantaneous concentration of radiation damage point defects is kept to a higher level than what exists in the samples analyzed after irradiation.

2.06.2.1 Parameters Acting at the Mesoscopic Scale

The effect of the parameters acting at the mesoscopic scale can be assessed using solutions of the heat equation obtained for particular microstructures, for instance, a matrix containing inclusions.

2.06.2.1.1 Porosity and grain boundaries

The porosity existing in fresh fuels evolves during irradiation and has a strong impact on the heat transfer in the pellet because of its low thermal conductivity as compared to the solid. The porosity is assumed to have identical effects on the fresh and irradiated fuels and therefore the same correction formulae are used. This assumption is valid when the shape of the pores is similar and the pore volume fractions are comparable (i.e., around 5 vol%). In order to analyze the effect of parameters other than the porosity, its effect is normalized to 0 or 5 vol% by converting the measurements obtained for samples with different porosity levels. Irradiation-induced pore-size distribution changes have a small effect, but the pore shape can play a larger role if the pores are not spherical and are oriented. The correction formulae are derived from composite material formulae giving the effective conductivity of a matrix containing inclusions,[4] often simplified by attributing zero conductivity to the pores. Loeb[5] introduced the effect of temperature to take into account the radiative heat transfer in the pores. The influence of the complex pore shape observed in irradiated fuel was investigated by Bakker using the finite-elements technique applied to realistic microstructures obtained by image analysis.[6] Usually the thermal conductivity is normalized to 5% porosity using simplified approaches, for instance the formula of Brandt and Neuer as recommended by Fink[7] (Eq. (2)).

$$\lambda_{95}(T) = \frac{1 - 0.05\, f(T)}{1 - P\, f(T)}\, \lambda_P(T) \tag{2}$$

where $f(T) = 2.6 - 0.5T/1000$, T is in °C and P is the porosity fractional volume.

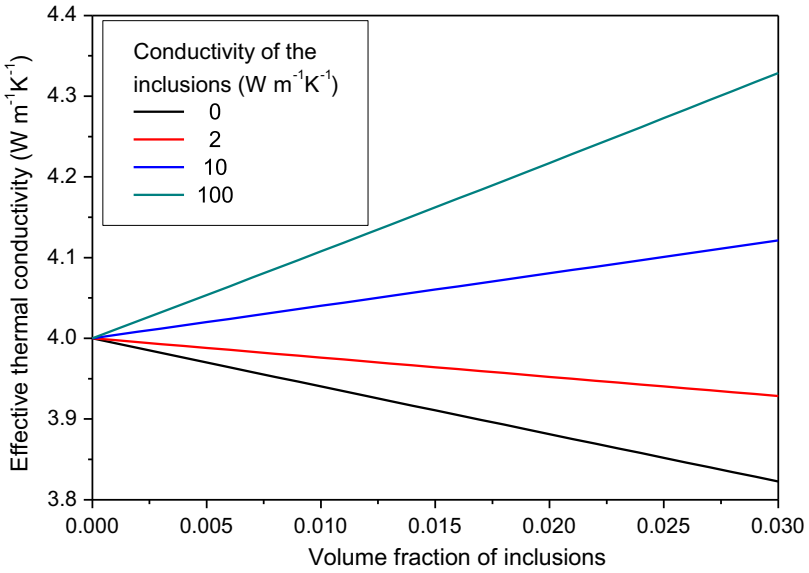

Fig. 3 Effective thermal conductivity for a solid composed of a matrix of conductivity 4 W m^{-1} K^{-1} containing inclusions of conductivities 0, 2, 10, and 100 W m^{-1} K^{-1}, determined with the model of Maxwell.[4]

2.06.2.1.2 Precipitates of insoluble fission products

Precipitates are formed by fission products that are insoluble in the UO_2 lattice. They form oxide inclusions (such as $BaZrO_3$ or $SrZrO_3$) or metallic inclusions (Mo, Ru, Tc, Rh, Te, Pd, Sn, Cd, Sb, Ag, etc.) and their influence on the effective thermal conductivity can be evaluated by the formulae obtained for composite materials[8]: for instance, the Maxwell–Eucken equation.[9] As the volume fraction of inclusions is small, this simple model gives results of sufficient accuracy. The inventory and volume fraction of the precipitates can be calculated from the number of moles created at a given burnup. For illustration purposes, the Maxwell–Eucken formula was applied at a fixed temperature assuming a UO_2 matrix with a thermal conductivity of 4 W m^{-1} K^{-1} containing inclusions with thermal conductivities of 0 (pores), 2 and 10 (ceramic precipitates), and 100 (metallic precipitates) W m^{-1} K^{-1}. As shown in Fig. 3, the effect of the precipitates on the thermal conductivity varies linearly with their volume fraction, which is proportional to the burnup, *bu*. If the coefficients *a* and *b* are used to describe this proportionality, we have $\lambda_k = a - b \times bu$; the negative burnup dependence is introduced because the fuel thermal conductivity globally decreases with burnup. Usually, the thermal conductivity is approximated by the $1/(A+BT)$ formula, where *A* and *B* describe the phonon scattering mechanisms. Therefore, one obtains the formula $A+BT = (1/a)/(1 - b/a \times bu)$ and if $b/a \times bu$ is small, we have $A+BT = 1/a + (b/a^2 \times bu) - (b^2/a^3 \times bu^2) + \ldots$. At a fixed temperature *T*, the *A* and *B* coefficients depend in a linear or quadratic way on the burnup. This kind of dependence is often found in thermal conductivity correlations.

2.06.2.2 Parameters Acting at the Atomic Lattice Scale

The fission products that form a solid solution with UO_2 and the point defects influence the thermal conductivity at the atomic scale. Their effect on the thermal conductivity is interpreted in terms of phonon scattering and is described by the formula $\lambda = 1/(A+BT)$.[8] The constant *A* can be expressed as the sum of the thermal resistance due to phonon scattering by substitutional atoms or point defects (impurities, interstitial atoms, vacancies) using the expression obtained by Ambegaoker.[10] The main parameters are the Debye temperature, the mean phonon velocity, and the phonon diffusion cross section of the defects. Extended defects such as grain boundaries scatter phonons by limiting their mean free path. The product *BT* corresponds to the intrinsic lattice thermal resistivity caused by phonon–phonon scattering. The value of *B* can be evaluated from a simplified model by Leibfried and Schlömann,[11] but the information available on the physical and thermodynamic data of UO_2 is not sufficiently accurate. Therefore, *B* is usually obtained empirically from the measured thermal resistivity slopes.

2.06.2.2.1 Soluble fission products

Actinides, rare earths, and transition metals can form mixed oxides with UO_2 or $(U,Pu)O_2$. Examples of these elements are the fission products Zr, Ce, Nd, Ba, La, Pr, Sr, Sm, Y, Rb, Te, Pu, Np.[12] Their solubility limits determined for binary systems are never reached in the case of irradiated fuel, and these elements can be completely or partially dissolved in the fuel matrix. When such solid solutions are formed, these atoms act as phonon scattering centers as a result of the differences in bonding potential, ionic radii, or mass between the impurities and the substituted atoms (U or Pu). The total scattering coefficient can be evaluated from the differences in atomic mass and ionic radii[13] and from the Grüneisen constant, which represents the strain generated in the lattice by the difference in ionic radius and is usually treated as an empirical parameter obtained from experimental data.[14–17]

2.06.2.2.2 Volatiles and fission gases

Insoluble or volatile fission products (Kr, Xe, Cs, Te, I, etc.) are partially dispersed as interstitials and induce static displacements of host lattice atoms U or Pu from their mean lattice sites. In that case, their effect can be interpreted with the same equations as for the dissolved fission products. The fission gas, thermodynamically insoluble in the matrix, is initially injected into the lattice and may precipitate into bubbles. Since collisions with fission fragment recoil cascades tend to re-inject gas into the lattice, for temperatures below about 1100K, a fraction of the gas is kept in dynamical solution. At higher temperatures, most of the gas precipitates into bubbles or pores or can be released from the pellet. The simultaneous mechanisms of gas diffusion, precipitation, and release can be described by reaction-rate equations[18] to calculate the partitioning of the gas in the different states starting from a number of kinetic (gas creation rate, diffusion coefficient, and resolution rate) and structural (grain size, radii, and concentrations of the bubbles) parameters. The entire irradiation history of the sample and, when laboratory annealing is involved, the applied temperature program, have to be considered.

2.06.2.2.3 Point defects created by radiation damage

The perturbations of the crystal lattice due to the displacement of atoms, that is point defects (interstitials, vacancies) and extended defects (defects clusters, dislocations, voids), contribute to the degradation of the thermal conductivity by scattering or limiting the mean free path of the phonons. This perturbation at the atomic scale is of the same nature as for soluble fission products and is also interpreted in terms of phonon scattering centers. Two aspects introduce uncertainties into the prediction of the effect of radiation damage: the concentration is difficult to calculate as a function of the irradiation conditions and the effect on the thermal conductivity is nonlinear (saturation occurs). Because of the large number of displacements produced by fission, the point defect concentration is expected to saturate early, probably before a burnup of 1 MWd kg HM^{-1}, the saturation level depending on temperature. Supplementary radiation damage of a dynamical nature is present only in pile because of the fission spikes and its concentration depends on the fission rate; it disappears immediately when irradiation stops.

2.06.2.2.4 Stoichiometry

Stoichiometry has a major effect on the thermal conductivity of fresh fuels.[19] UO_2 is generally stoichiometric when introduced in pile and the O/U ratio of UO_2 irradiated under LWR conditions remains close to 2.00 up to a burnup of 100 MWd kg HM^{-1}.[20–22] This parameter is, however, difficult to define for an irradiated fuel because of the complex chemical composition. Also, the effect of the oxygen defects due to the nonstoichiometry can be expected to be reduced because of the large number of oxygen defects created by irradiation.

2.06.2.2.5 Additives in UO_2 (Pu, Gd, Cr)

The addition of Pu, Gd, or Cr to UO_2 reduces the thermal conductivity of the fresh fuel. While the concentrations of Pu and Gd are of a few percent, these are only of a few hundreds of ppm for Cr. These additives may form solid solutions with UO_2 or be present as precipitates. The perturbation decreases with burnup because of the other burnup effects, as observed for $(U,Gd)O_2$ by Sonoda *et al.*,[23] for $(U,Pu)O_2$ by Fujii *et al.*,[24] and Cozzo *et al.*,[25] and for Cr by Caillot *et al.*[26]

2.06.2.3 Global Parameters

Because of the complex characteristics of the irradiated fuel, the thermal conductivity is often deduced from correlations using global parameters summarizing the state of the fuel: for instance, the burnup and the irradiation temperature. Some fuel characteristics are implicitly taken into account.

2.06.2.3.1 Irradiation temperature

The irradiation temperature has an impact on the state of the fuel. During long irradiations, temperature has an effect on the microstructure of the fuel and on the concentration of radiation damage accumulated. During a short annealing (transient or laboratory annealing), the effect is mainly restricted to the radiation damage concentration change and to the redistribution of some fission products: precipitation of atoms that were distributed as single atoms including the formation of fission gas bubbles. However, the definition of this parameter is vague because the irradiation temperature at a given radial position is not constant throughout the irradiation and the real relevant parameter is the irradiation temperature history. Some properties like the fission gas release need to be determined considering the whole irradiation temperature history, while other characteristics like the radiation damage point defects concentration depend mainly on the irradiation temperature at end of life (EOL).

2.06.2.3.2 Plutonium distribution (MOX microstructure)

The fresh fuel plutonium concentration and distribution (homogeneous or heterogeneous microstructure) and the induced variations in the local stoichiometry are supplementary parameters for MOX fuels. The plutonium concentration decreases with burnup whereas it increases in UO_2. Therefore, the differences observed in fresh fuels linked to the plutonium effect can be expected to decrease with burnup, at least for homogeneous MOX fuels. In heterogeneous MOX, the microstructure may have an enhanced impact because of the presence of Pu-rich agglomerates in which the burnup is much higher than in the matrix. However, recent studies showed that this effect is in fact negligible.[27,28]

2.06.2.3.3 Microstructure

The microstructure of the fuel is linked to the presence of additives and porosity, voids, and fission gas bubbles, their concentrations changing with the radial position. Other parameters concern the fuel matrix itself: the densification at the beginning of life and the grain size evolution. The effect of porosity and voids can be approximated by applying a factor to the matrix conductivity, determined for instance by the formula of Maxwell giving the effective thermal conductivity λ_{eq} of a medium constituted by a matrix of conductivity λ_m containing a small volume fraction v_f of inclusions having a conductivity λ_f (Eq. (3)). This approximation is obtained only when $\lambda_m \gg \lambda_f$, and is therefore not usable for ceramic or metallic precipitates. Approximate formulae, validated for porosity in nuclear fuels, were proposed by Brandt and Neuer.[29]

$$\lambda_{eq} = \lambda_m \frac{\lambda_f + 2\lambda_m + 2v_f(\lambda_f - \lambda_m)}{\lambda_f + 2\lambda_m + v_f(\lambda_m - \lambda_f)} \underset{if\ \lambda_m \gg \lambda_f}{=} \lambda_m \frac{2(1 - v_f)}{2 + v_f} \tag{3}$$

The macroscopic cracking and fracture of the pellet are heterogeneities that cannot be taken into account for the definition of an equivalent thermal conductivity because their size (several mm) is not small compared to the size of the pellet (no separation of scales exists between the volume over which the effective thermal conductivity is evaluated and the size of the pellet). Cracking can be separated into radial and tangential, the latter decreasing the apparent thermal conductivity.

Extensive microstructure changes take place with the formation of the HBS starting from the periphery of the pellet for discharge burnups higher than about 40 MWd kg HM^{-1} or local burnups higher than about 60 MWd kg HM^{-1}. This structure is characterized by a reduced grain size, an increase in porosity, the formation of metallic fission product precipitates and a depletion of fission gas from the UO_2 matrix.[30,31]

2.06.2.3.4 Burnup

The fuel burnup reflects the proportion of fissioned atoms and is the most commonly used parameter for the interpretation of thermal conductivity degradation. In principle, this parameter integrates the phenomena that do not depend on the irradiation conditions, that is, the concentration of nonvolatile fission products. In practice, it is often the only parameter of the correlations and is used to account for (almost) all irradiation effects. Some particular effects exist at low burnup: the fast buildup of irradiation damage, and at high burnup: the formation of the HBS.

2.06.2.4 Necessary Reduction of the Number of Parameters

The fuel thermal conductivity changes during irradiation as a result of fission and high operating temperatures; the chemical composition, lattice structure, and microstructure evolve in a complex and correlated manner. The fuel microstructure and state result from the irradiation history (transients generate cracking, shutdown periods result in autoirradiation at low temperatures, etc.). A complete and three-dimensional knowledge of the fuel characteristics is required for the prediction of the thermal conductivity. The number of parameters is large and it is difficult to isolate and model their effects individually. Furthermore, many parameters act in a coupled manner: that is, the impact of the individual parameters is not the sum of the individual effects. Therefore, no purely theoretical model is available and semiempirical correlations are built from the interpretation of experimental results by selecting the most influential parameters, the effect of the others being implicitly included when the models are adjusted to measurement results.

Two categories of parameters can be distinguished: first, the parameters that depend on burnup but not on irradiation conditions. The burnup is a global parameter that integrates all the effects which are proportional or related to it only, for instance, the concentration of soluble fission products or precipitates. Second, the parameters are those that depend on burnup and irradiation temperature history. This is the case for radiation damage, for the state of fission products that are present as isolated atoms and can precipitate, or for the distribution of volatile fission products between the states dynamically dissolved, precipitated in bubbles or pores, or released.

The proposal of a model implies a reduction in the number of parameters remaining, for instance, only the burnup or a second parameter summarizing the effect of the irradiation history, such as the irradiation temperature[1] or the lattice parameter,[32] assuming that these parameters describe, with sufficient precision, the state of the fuel.

The general expression of the heat conduction used for irradiated fuels is similar to the one adopted for the fresh fuel (Eq. (4)). It includes the lattice conduction mechanism by phonons, empirically represented by $1/(A + BT)$ and largely dominant up to temperatures of about 1600K, and the high-temperature contribution attributed to the electron vacancy pair mobility, usually represented by adding an expression of the form $C\,e^{DT}$. This last contribution cannot be accurately quantified because of the lack of measurements at high temperatures, both for fresh and for irradiated fuels.

$$\lambda = \frac{1}{A + BT} + C\,e^{DT} \tag{4}$$

The quantity $1/A + BT$ applies only to perturbations at the atomic scale, that is, the effects of soluble fission products, and to point defects (radiation point defects, nonstoichiometry, dynamically dissolved atoms and fission gases). It is not rigorous for precipitates and porosity, as the effect of these parameters is macroscopic and described by composite materials formulae derived from the solution of the Fourier law. In practice, this formalism is often applied, including the effect of all the parameters. Fuel

variants, such as $(U,Gd)O_2$, UO_2 doped with Cr, or MOX, are modeled on the basis of UO_2, with supplementary parameters describing the effect of the additive.

2.06.3 Specific Heat of Irradiated Fuel

Specific heat is an important parameter for the transient behavior studies where the temperature variations are linked to the variations of reactor power. Also, it is required for the calculation of thermal conductivity from thermal diffusivity. Only a very limited number of studies are available and the specific heat of irradiated fuel is not yet fully clarified. The effects of soluble fission product elements added to fresh UO_2 were quantified, for instance, by Verall and Lucuta,[33] Matsui *et al.*,[34] and Takahashi and Asou.[35] No large burnup effect was found because the specific heat obeys the law of mixtures (Neumann–Kopp law) and because only a limited fraction of the fresh fuel heavy metal atoms change nature during irradiation.

Specific heat measurements for irradiated fuel by calorimetric techniques show an exothermic effect during the first heatup of the sample linked to the recombination of radiation damage and to fission products redistribution. The apparent specific heat is lower than for annealed samples because of the heat effect, as observed by Gomme *et al.*[36] and Yagnik and Turnbull.[37] A similar effect is observed for $(U,Pu)O_2$ samples damaged by autoirradiation.[38] This means, for instance, that during fast power increases, the temperature will increase faster than predicted using the fresh fuel-specific heat. For the intrinsic specific heat (i.e., measured on annealed samples), no significant difference was found when compared with fresh fuel. Similar results were obtained by direct measurements of specific heat on irradiated fuels by laser flash, reported by Ronchi *et al.*[1] for UO_2 and by Sonoda *et al.*[23] for $(U,Gd)O_2$. Therefore, the specific heat of irradiated fuel is generally assumed to be equal to that of the fresh fuel.

2.06.4 Thermal Conductivity of Fuels With Simulated Burnup Effects

The changes in the fuel thermal conductivity were quantified in simulated irradiated fuel (SIMFUEL) in which additives are introduced in UO_2.[39] Some additives are soluble in the lattice and other precipitate as second phases. The advantage of this approach is that the samples are easy to prepare and handle. Single effects can be studied, but the main disadvantage is that only part of the burnup effects can be simulated. This approach was used, for instance, by Ishimoto *et al.*[15] for UO_2 and $(U,Gd)O_2$ and by Kang *et al.*[40] for UO_2. Hartlib *et al.*[41] simulated the effects of fission products in MOX fuel and evaluated the decrease in thermal conductivity, and this work was used by Philipponneau to obtain a thermal conductivity correlation for the irradiated fast reactor MOX.[42]

The most complete work on simulated burnup effects was published by Lucuta *et al.*,[39] who proposed a formula in a form of factors contributing to the degradation of the thermal conductivity λ_0 of unirradiated UO_2 (Eq. (5)).

$$\lambda_{95} = \lambda_1(bu) \cdot \lambda_2(p) \cdot \lambda_3(x) \cdot \lambda_4(r) \cdot \lambda_0 \tag{5}$$

In this formula, $\lambda_1(bu)$ is the burnup dependence, containing the effect of dissolved fission products as derived from measurements on SIMFUEL, and the effect of precipitates, assessed theoretically with composite materials formulae, including a correction reflecting that precipitation takes place at high temperature. $\lambda_2(p)$ accounts for the porosity and bubbles contribution, based on the Maxwell–Eucken formula for composite materials. $\lambda_3(x)$ refers to the effect of nonstoichiometry and was assessed from SIMFUEL measurements results, but this factor is generally not used as the fuel is assumed to be stoichiometric. $\lambda_4(r)$ describes the radiation damage effect presuming that recovery takes place progressively in the range 600–1200K. This model was used in some fuel performance codes[43] but was replaced[44] because its predictions were found to be too high.

2.06.5 Thermal Conductivity Determined From In-Pile Measurements

The fuel thermal conductivity can be deduced from a measurement of the temperature history at the pellet center with a thermocouple during irradiation. The determination is done for different values of the reactor power and assuming that the coolant temperature and the fuel-cladding gap conductance are known. In order to suppress the uncertainties linked to the heat transfer in the fuel-cladding gap, some rig designs include simultaneous central and off-central temperature measurement positions. The fuel center temperature is linked in an integral way to the radial profiles of the thermal conductivity and the heat production (Eq. (1)).

The advantages of this approach are that the determination includes the effect of the dynamical damage created by the fission rate. Also, in contrast to out-of-pile measurements usually carried out a few years after the end of the irradiation, the measurement is not perturbed by the out-of-pile autoirradiation damage accumulated during storage. The disadvantages include the uncertainties linked to the fuel-cladding heat transfer and the fact that it is an integral measurement only, not local. Also, the criteria for the definition of an equivalent thermal conductivity are not perfectly fulfilled because the heat sources are not homogeneously distributed within the material; the heat production is a function of the radius, and in MOX fuel, it is concentrated in the Pu-rich agglomerates.

The main result was obtained by the Halden Reactor Project. The thermal conductivity of irradiated UO_2 (Eq. (6)) is given by Wiesenack.[45] A recent adaptation (Eq. (7)) was cited by Lanning *et al.*,[44] including the effect of gadolinia. T_c is the

current temperature in °C, *bu* is in MWd kg HM^{-1}, *gad* is the weight fraction of gadolinia, and ϑ is the lower value between T_c and 1650°C.

$$\lambda_{95} = \frac{1}{0.1148 + 3.05 \cdot 10^{-3} \cdot BU + 2.475 \cdot 10^{-4}(1 - 3.3 \cdot 10^{-3} \cdot BU)T_C} + 0.0132e^{0.00188 \cdot T_C} \quad (6)$$

$$\lambda_{95} = \frac{1}{0.1148 + 1.1599 \cdot gad + 4 \cdot 10^{-3} \cdot BU + 2.475 \cdot 10^{-4}(1 - 3.3 \cdot 10^{-3} \cdot BU)\vartheta} + 0.0132e^{0.00188 \cdot T_C} \quad (7)$$

Lee *et al.*[46] proposed to adapt the correlation to take into account the increased porosity in the HBS (Eq. (8)) by using a formula for composite materials derived from a one-dimensional heat transfer approximation made by Kampf and Karsten.[47] In Eq. (8), λ_0 is the conductivity of the fully dense matrix, λ_p is the conductivity of the pores, and P_{rim} is the volume fraction of pores in the HBS.

$$\lambda_{rim} = \lambda_0 \left\{ 1 - P_{rim}^{2/3} \left[1 - \frac{1}{1 + P_{rim}^{1/3} \left(\frac{\lambda_0}{\lambda_p} - 1 \right)} \right] \right\} \quad (8)$$

Wiesenack *et al.*[48] proposed an adaptation for MOX fuel also using Eq. (8) and considering a matrix with low Pu content of conductivity λ_0 and Pu-rich inclusions of conductivity λ_p. The thermal conductivity of the matrix is obtained by assuming that the effect of the plutonium is proportional to its concentration, while the conductivity of the Pu-rich inclusions is obtained with the correlation of Phillipponneau for fresh fuel.[42]

The Halden Reactor Project also developed an adaptation of their correlation for MOX fuel, based on fuel center temperature measurements. As cited and adapted by Lanning *et al.*,[44] this formula is obtained by multiplying the phonon term of the formula for UO_2 as given by Eq. (7) by the factor 0.92.

The conductivities for UO_2 (Eq. (6)), $(U_{0.95}Gd_{0.05})O_2$ (Eq. (7)), and LWR MOX (Eq. (7) multiplied by 0.92) fuels are plotted in **Fig. 4** as a function of burnup. It can be seen that the conductivity of UO_2 and $(U_{0.95}Gd_{0.05})O_2$ converge with increasing burnup. The constant ratio between the UO_2 and MOX thermal conductivities is a matter of discussion. Convergence between UO_2 and MOX was proposed by other authors, for instance, from in-pile central temperature measurements by Fujii *et al.*,[24] who made the analysis with the assumption that the burnup degradation for MOX is slightly lower than that of UO_2. A recent investigation based on fuel central temperatures measurements found that the thermal conductivity of MOX could be higher than that of UO_2 at the high burn-up of 74 MWd kg HM^{-1},[49] due to the differences in soluble fission products generated and to a higher mobility of Pu and oxygen in MOX which promotes the recovery of irradiation point defects. Other correlations were obtained on the basis of in-pile measurements, for instance,[50] using a database of central temperature measurements combined with the radiation damage term derived by Lucuta *et al.*[39]

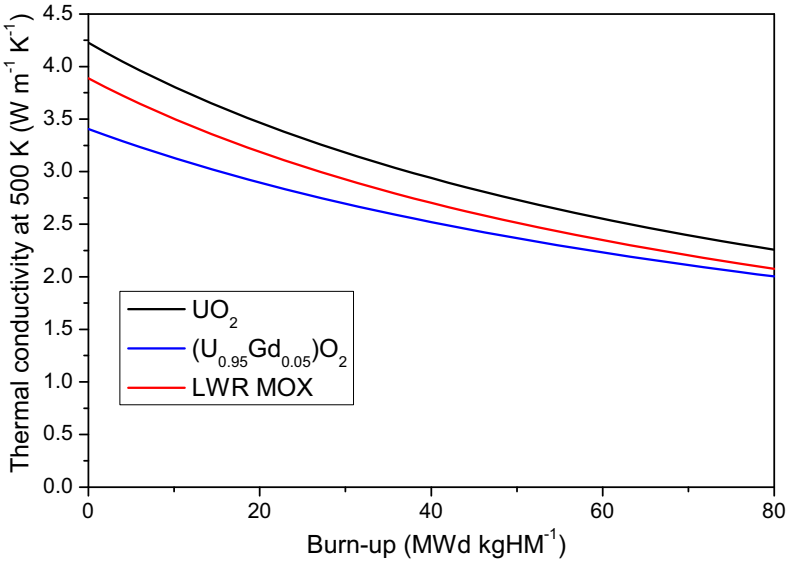

Fig. 4 Thermal conductivities of UO_2,[44] $(U_{0.95}Gd_{0.05})O_2$,[43] and LWR MOX[43] predicted by models based on in-pile measurements. Irradiation temperature 500K.

2.06.6 Thermal Conductivity Out-of-Pile Measurement on Irradiated Fuel

In this technique, the irradiated fuel samples are small disks or disk fragments with irregular shape and are not suitable for direct measurements of thermal conductivity. Out-of-pile measurements of the thermal diffusivity are carried out using shielded laser flash devices, specially designed and constructed for irradiated nuclear fuel, for instance, at AEA technology,[36] at NNFD,[51] and at JRC.[52] The samples are disks or fragments of a disk having plane and parallel faces, with a thickness of about 1 mm, and with diameters or lateral dimensions between 3 mm and the pellet diameter. The sample is first heated up to the measurement temperature. Then, one face receives a heat pulse produced by a laser and the temperature rise at the opposite face is recorded as a function of time to deduce the thermal diffusivity. The thermal conductivity $\lambda(T) = \rho(T)C_p(T)\alpha(T)$ is then calculated from the thermal diffusivity $\alpha(T)$, the specific heat $C_p(T)$, and the density $\rho(T)$.

The advantages of this technique are that it is a direct measurement not requiring assumptions about other parameters and a uniform temperature of the sample; samples can be chosen free of cracks, measurements can be made at different radial positions, and annealing studies can be carried out to investigate the radiation damage recovery. Some experimental difficulties arise because of the delicate sample preparation procedure and their brittleness. From the point of view of the relevance in terms of in-pile behavior, drawbacks include the absence of a thermal gradient in the sample (the irradiation temperature has a unique and different value in each radial position) and the absence of the dynamical damage produced and maintained in-pile by fission. Because of the supplementary damage created during storage, the interpretation requires an analysis of autoirradiation effects and annealing of in-pile damage. These drawbacks are avoided when the thermal conductivity is evaluated in pile using thermocouples, but then supplementary uncertainties arise because of the integral nature of such measurements.

2.06.6.1 Measurement Procedure and Analysis of the Results

A typical experiment usually starts at a low temperature (300–500K) and thermal diffusivity measurement cycles are recorded with increasing maximum temperatures. An increase in thermal diffusivity is observed after the annealing cycles, the magnitude of which depends on the maximum temperature reached. Therefore, a typical thermal diffusivity measurement does not result in a unique curve as a function of temperature but in a series of curves obtained by increasing the maximum measurement temperature. Even after high temperature annealing, recovery is only partial because some burnup effects remain, and the value corresponding to unirradiated UO_2 is not obtained. The typical evolution of the thermal conductivity during successive annealing cycles is presented in **Fig. 5** for a sample having a burnup of 30 MWd kg HM^{-1} and an irradiation temperature of 900K.[1]

The in-pile microstructure and radiation damage concentration result from an equilibrium between the defect creation rate due to fission and their recombination or migration rates which depend on temperature. The point defect equilibrium concentration corresponds to the saturation level at the irradiation temperature. For out-of-pile measurements at a specific temperature below the irradiation temperature, the damage concentration at this measurement temperature is lower compared to that of a sample that would have been irradiated at this temperature, and the microstructure is different. This is particularly obvious for samples where the HBS has formed, this structure having properties different from the unrestructured fuel and forms only at low irradiation temperatures. For out-of-pile measurements above the irradiation temperature, it is not clear whether the damage concentration is higher or lower compared to a sample that would have been irradiated at these temperatures. Thus, only the measurements at the irradiation temperature represent the in-pile state of the fuel, as discussed by Beyer and Lanning.[53] This statement assumes that autoirradiation effects can be neglected: for instance, if the measurement takes place immediately after the irradiation or if the fuel

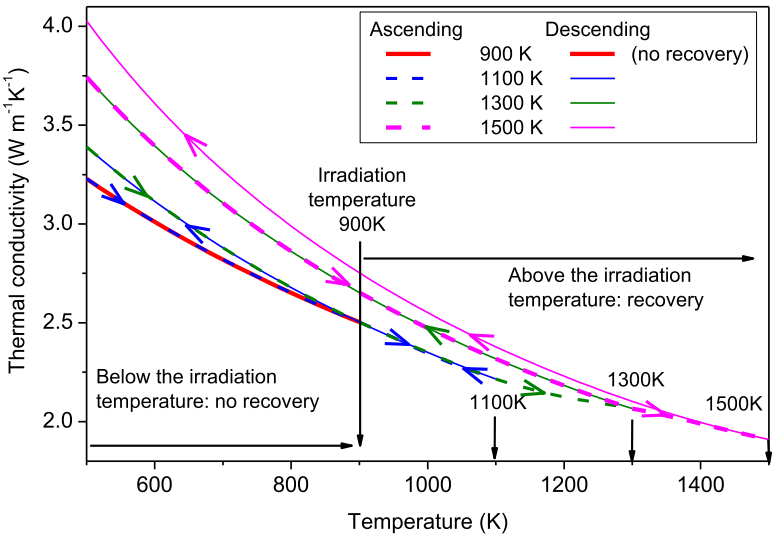

Fig. 5 Thermal conductivity of a UO_2 sample with a burnup of 30 MWd $kgHM^{-1}$ and an irradiation temperature of 900K, measured during four successive out-of-pile annealing cycles with increasing maximum temperatures. As autoirradiation damage was not present, recovery begins after the irradiation temperature is exceeded.

α-activity is low. The effect of the autoirradiation can be quantified by measuring the magnitude of the recovery at temperatures below the irradiation temperature. In the absence of autoirradiation effects, no recovery will take place, as illustrated in Fig. 5.

When the experimental measurements are interpolated by the $1/(A+BT)$ equation, a clear distinction exists between the ascending temperature regimes, where recovery takes place and therefore A and B change during the measurement as some characteristics of the sample being measured change, and the descending temperature regimes, where A and B have constant values.

Generally, the samples are resistant to fracture up to the irradiation temperature and then they may fracture or loose fragments. Fracture resistance at higher temperatures depends on the burnup and microstructure of the sample (high burnup samples with the HBS structure are less resistant), but also has a stochastic nature linked to the existence of cracks.

2.06.6.1.1 Underlying mechanisms of the recovery

The annealing cycles measurement procedure is used to investigate the recovery mechanisms and also to accumulate sufficient data that will be used later to deduce the thermal conductivity at the irradiation temperature; this temperature being not necessarily known at the moment when the measurements are done or is to be assessed using the experimental results.

Most of the recovery is due to a decrease in the concentrations of point defects, voids, and dislocations (recombination or precipitation). As discussed by Ronchi *et al.*,[1] a contribution is also due to the redistribution of fission product atoms, for instance, the precipitation of isolated atoms or the formation of fission gas bubbles from dynamically dissolved atoms present at the end of the irradiation. The mechanisms responsible for the out-of-pile annealing behavior are not fully described by a quantitative interpretation. Their investigation is, however, important for the understanding of the relation between the irradiation temperature and the in-pile state of the fuel. Studies of α-doped fuels have shown that the recovery takes place in different steps as a function of the annealing temperature. The different annealing stages and the nature of the related defects were shown to be identical in autoirradiated and reactor-irradiated fuels;[38] these stages are the oxygen vacancy/interstitial recombination (oxygen Frenkel pairs) at 600–800K, the recombination of uranium vacancy/interstitial clusters at 800–1000K, dislocation loop formation, and precipitation of bubbles near 1200K.

Annealing time, that is, the hold time of the sample at the annealing temperature, was not found to have a measurable effect on the thermal diffusivity as observed by Ronchi *et al.*[1] and Carrol *et al.*[54] However, this result is not necessarily general, because the thermal diffusivity is not measured during the stabilization of the measurement temperature which is relatively long, and the annealing durations are limited for practical reasons.

2.06.6.1.2 Autoirradiation effects

The thermal diffusivity values obtained during laboratory measurements, performed a few years after the end of the irradiation, are not the same as the EOL values since they include the effect of supplementary damage produced by autoirradiation during storage. The impact of autoirradiation depends on the storage time, the initial enrichment of the fuel, and the burnup. Quantitative studies on fresh α-doped fuels have provided correlations between the autoirradiation dose and the thermal conductivity degradation, and have shown that the effect of radiation damage on the thermal conductivity saturates at a lower displacements per atom (dpa) value than other properties, for instance, the lattice parameter.[38] These studies are, however, not directly applicable to irradiated fuels, because such fuels are already damaged when autoirradiation begins, and the extent of this initial damage is not yet quantified in terms of damage concentrations.

Three characteristic thermal conductivity curves can be distinguished (Fig. 5):

(1) The first curve represents the conductivity measured on increasing the temperature up to the irradiation temperature. During this stage, only damage produced by the out-of-pile autoirradiation is annealed.
(2) The recovered conductivity is given by the curve obtained during the descending temperature measurement made after this annealing. This corresponds to the first part of the second curve, when the measurement begins at low temperature and continues up to temperatures higher than the irradiation temperature. During this stage, the damage produced in pile is progressively annealed above the irradiation temperature.
(3) The third curve represents the conductivity of the sample after annealing at the maximum measurement temperature.

This interpretation supposes that the damage produced by autoirradiation can be clearly distinguished and separated from that produced in pile. In fact, both are of a similar nature but are produced at different temperatures.

In pile, damage that can be removed at temperatures lower than the irradiation temperature is immediately healed. At EOL, a sample can be assumed to have a concentration of radiation damage corresponding to the saturation level at the irradiation temperature. This damage is annealable only at temperatures higher than the irradiation temperature. During storage, the damage concentration increases and reaches the saturation levels at the storage temperature. As autoirradiation produces damage of identical nature to in-pile damage, part of this damage can recover at temperatures below the irradiation temperature, and part at temperatures above it. This last contribution requires supplementary modeling work.

2.06.6.2 Summary of the Main Experimental Results

Two categories of approaches can be distinguished: studies on fuel irradiated under standard conditions with irradiation temperature and burnup gradients existing between the pellet center and periphery; and studies of special irradiations, where almost uniform irradiation temperature and burnup are obtained.

Table 1 Some out-of-pile thermal diffusivity measurements from which the thermal conductivity of irradiated fuel has been determined

Author and reference	*Year*	*Fuel*	*Irradiation*	*Burnup (MWd kg HM^{-1})*	*Meas. temp. range (K)*	*Comment*
Yamamoto *et al.*[60]	1993	$(U_{0.82}Pu_{0.18})O_2$ FBR	Standard	8, 19, 35	850–1900	No burnup degradation observed
Carrol *et al.*[54]	1994	UO_2	Standard	40	670–1670	Two samples, two runs each
Gomme *et al.*[36]						
Ohira and Itagaki[55]	1997	UO_2	Standard	61	670–1794	One cycle
Hirai[51]	1998	UO_2	Standard	39		Irradiation with a temperature escalation at 1270K and then 18 days at 573K
Baron[32]	1998	UO_2	Capsule	28, 39, 63, 80	300–1900	Two or more cycles per sample
Yagnik[62]	2000	$(U,Gd)O_2$		21, 47		
Nakamura[56]	1998	UO_2	Standard	63	Three or four cycles	
Minato *et al.*[57]	2001	UO_2	Capsule	18, 39	380–1780	Two cycles
		$(U,Gd)O_2$		39		
Amaya *et al.*[58]	2002	UO_2 same as Hirai[50]	Standard	39, 60	465–1890	Three cycles
		$(U,Gd)O_2$		43, 50		
Ronchi *et al.*[1]	2004	UO_2	Capsule	34, 52, 76, 92	500–1500	Ten samples
Kinoshita *et al.* [63]						
Walker *et al.*[59]	2006	UO_2	Standard	102	500–1100	Two samples, three radial positions
Sonoda *et al.*[23]	2007	UO_2 same as Ronchi *et al.*[1]	Capsule	32, 53, 86, 96	500–1500	Summary of HBRP results
		$(U,Gd)O_2$		32, 53		
Cozzo *et al.*[25]	2010	$(U,Pu)O_2$ LWR	Standard	33	500–1550	Three radial positions
Staicu[61]	2011	$(U,Pu)O_2$ LWR	Standard	23,42,47	500–1550	SBR and MIMAS MOX
Staicu[64]	2014	$(U,Gd)O_2$	Capsule	34, 52, 76, 92	500–1550	HBRP results

Experimental results obtained on standard fuels are summarized in **Table 1**. Measurement on UO_2 were published by Carrol and coworkers,[36,54] Ohira and Itagaki,[55] Hirai,[51] Nakamura,[56] Minato *et al.*,[57] Amaya *et al.*,[58] and Walker *et al.*[59] Amaya *et al.*[58] also investigated $(U,Gd)O_2$ with a burnup of 43.5 and 50.7 MWd kg HM^{-1}. Only a limited number of publications are available for MOX fuel. Measurements were published for homogeneous LWR MOX with burnups of 35[25] and 44 MWd kg HM^{-1}[61] and for heterogeneous MOX with burnups of 23 and 44 MWd kg HM^{-1}.[61] A comparison between the MOX of homogeneous and heterogeneous microstructures for the burnup of 44 MWd kg HM^{-1}[61] showed no significant difference. Also, no difference between irradiated LWR UO_2 and MOX was observed at the burnups of 35 and 44 MWd kg HM^{-1}.[61]

Yamamoto *et al.*[60] made measurements on FBR MOX with 17.7 wt% Pu and burnups of 8, 19, and 35 MWd kg HM^{-1} and did not observe a clear burnup dependence. This surprising behavior might be due to a low conductivity in the fresh fuel because of the high Pu content and of the hypostoichiometry, and also to measurement uncertainties. Another explanation could be a less than expected thermal conductivity degradation in FBR fuel due to the high irradiation temperature, to the redistribution and precipitation of fission products, to the high fission gas release and to the evolution of the stoichiometry. Yamamoto also measured the recovery behavior of a very low burnup fuel (0.5 MWd kg HM^{-1}) of high Pu content (28.8 wt%).

The studies on standard fuel are the most relevant but the effect of individual parameters is difficult to assess and usually only a small number of samples is considered, making the development of a thermal conductivity model problematic.

In the special irradiation NFIR (Nuclear Fuel Industry Research) and HBRP (High Burnup Rim Project), the samples were placed in metallic capsules to have an almost uniform irradiation temperature (**Table 1**). A flat burnup profile was achieved by a high enrichment of ^{235}U: 25.8% for HBRP and 19.8% for NFIR.[65] These irradiations involve a large number of samples of different burnups and irradiation temperatures, making them more suitable for the development of models. Despite the absence of a temperature gradient and of mechanical constraint induced by the cladding, comparative studies have shown good agreement between standard and special irradiation data[1,59] and also between the NFIR and HBRP data.[65] NFIR results were published by Baron[32] for UO_2 with burnups of 28, 39, 63, and 80 MWd kg HM^{-1} and by Yagnik[62] for UO_2 (similar to Baron[32]) and $(U_{0.9}\ Gd_{0.1})O_2$ for the burnups of 21 and 47 MWd kg HM^{-1}. HBRP results were published by Kinoshita *et al.*,[65] Ronchi *et al.*,[1] and Sonoda *et al.*[23] for UO_2 with burnups of 34, 52, 76, and 92 MWd kg HM^{-1} and different irradiation temperatures, and by Sonoda *et al.*[23] for $(U_{0.95}\ Gd_{0.05})O_2$ with burnups of 33 and 53 MWd kg HM^{-1}.

Results obtained by Carrol *et al.*,[54] Hirai,[51] Minato *et al.*,[57] and Baron[32] for UO_2 at a burnup of about 40 MWd kgHM^{-1} are shown in **Fig. 6**. The experimental points include the results of annealing cycles made to observe the out-of-pile recovery. The thermal conductivity measured at 500K ranges from about 2.8–4.8 W m^{-1} K^{-1}. This scatter is due to the differences in the experimental procedure (out-of-pile annealing history) and the irradiation temperatures, which are not always reported or considered as parameters. Such scatter is also observed for the results obtained by Ohira and Itagaki,[55] Nakamura,[56] Amaya *et al.*,[58] and Baron[32] for UO_2 at a burnup of about 60 MWd kg HM^{-1}, shown in **Fig. 7**. Compared with the measurements at about 40 MWd kg HM^{-1}

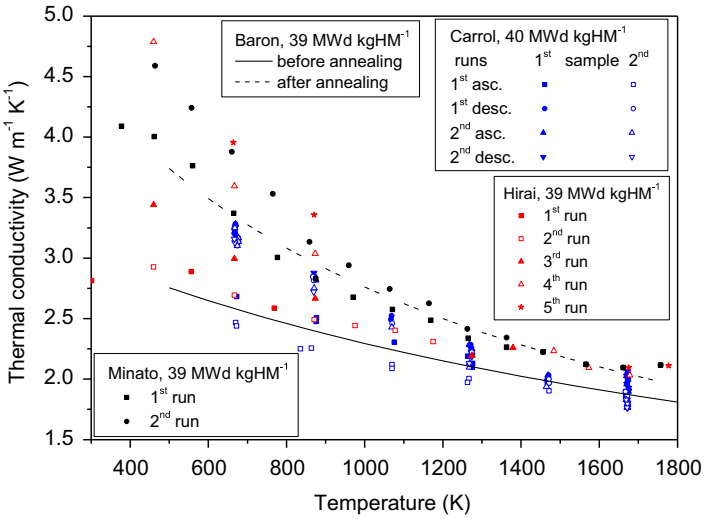

Fig. 6 Comparison of the thermal conductivity data published by Carrol *et al.*,[54] Hirai,[51] Minato *et al.*,[57] and Baron[32] for UO_2 with a burnup of about 40 MWd kg HM^{-1} (95% TD).

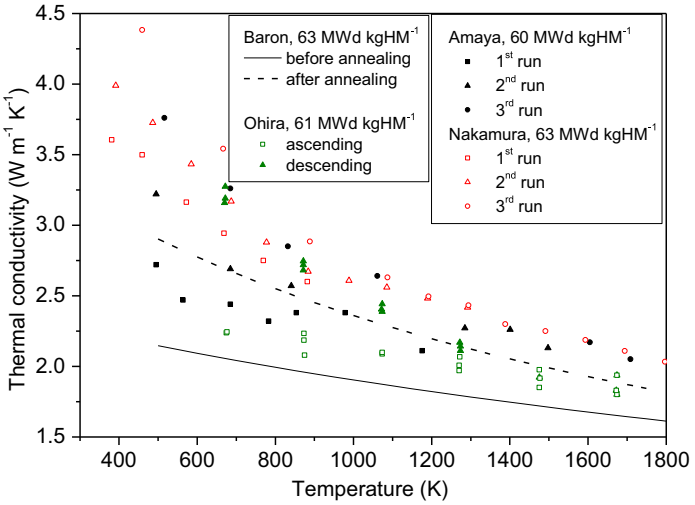

Fig. 7 Comparison of the thermal conductivity data published by Ohira and Itagaki,[55] Nakamura,[56] Amaya *et al.*,[58] and Baron[32] for UO_2 with a burnup of about 60 MWd kg HM^{-1} (95% TD).

(**Fig. 6**), a clear decrease is observed: for instance, at 500K, the thermal conductivity at a burnup of 60 MWd kg HM^{-1} ranges from 2.1 to 4.0 W m^{-1} K^{-1}.

Some results for $(U,Gd)O_2$ by Amaya *et al.* (6.4 at% Gd),[58] Yagnik (10 at% Gd),[62] and Sonoda *et al.* (5 at% Gd)[23] are shown in **Fig. 8**. The measurements of Yagnik show a clear degradation between the burnups of 21 and 47 MWd kg HM^{-1}. The thermal conductivity results of Amaya at burnups of 43.5 and 50.7 MWd kg HM^{-1} are in the same range as those of Yagnik at 21 and 47 MWd kg HM^{-1}, whereas the measurements of Sonoda at 52 MWd kg HM^{-1} are significantly lower.

The plots in **Figs. 6–8** illustrate the relatively wide range of thermal conductivity values obtained for a given burnup and temperature. In this context, the modeling assumptions used for the interpretation of the experimental results have a significant influence on the predicted in-pile thermal conductivity. The main models developed from out-of-pile results will be presented in the subsequent sections.

2.06.6.3 NFI (1997–2005)

Ohira and Itagaki[55] proposed the "NFI" (Nuclear Fuel Industries) model (Eq. (9), **Table 2**) for the thermal conductivity, based on experimental results for an UO_2 fuel with about 61 MWd kg HM^{-1}. A linear dependence of the parameter A on burnup was

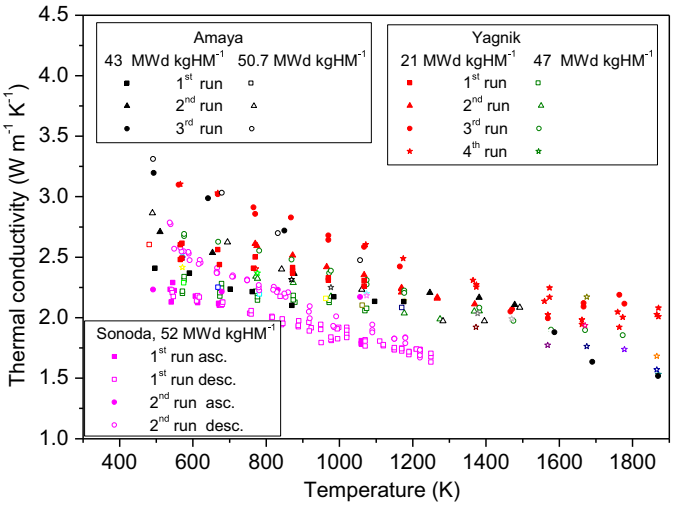

Fig. 8 Comparison of the thermal conductivity data for $(U,Gd)O_2$ published by Yagnik,[62] Amaya *et al.*,[58] and Sonoda *et al.*[23] (95% TD).

Table 2 Constants of the NFI and NFI-based models (Eqs. (9)–(11))

$a = 1.1599$	$A = 0.0452$ m K W^{-1}
gad: weight fraction of gadolinia	$B = 2.46 \times 10^{-4}$ m K W^{-1} K^{-1}
$f(bu) = 0.00187bu$: effect of FPs in solution in the matrix	$C = -5.47 \times 10^{-9}$ W m K^3
$g(bu) = 0.038bu^{0.28}$ effect of irradiation defects	$D = 13{,}520$K
$h(T) = 1/(1 + 396\exp(-6380/T))$: annealing of irradiation defects	$E = 3.5 \times 10^9$ W K m^{-1}
$x = 2.00 - O/M$ (O/M is the oxygen-to-metal ratio)	$F = 16{,}361$K
$A(x) = 2.85x + 0.035$ m K W^{-1}	$C_{mod} = 1.5 \times 10^9$ W K m^{-1}
$B(x) = (2.86–7.15x) \times 10^{-4}$ m W^{-1}	

assumed for the effect of fission products in solution, $f(bu)$, and the effect of radiation damage was modeled as increasing slowly with burnup (proportional to $bu^{0.28}$) and to be progressively annealed when temperature increases, as described by $h(T)$.

$$\lambda_{95} = \frac{1}{A + B \cdot T + f(bu) + g\,(bu)\,h\,(T)} + C \cdot T^2 + D \cdot T^4 \tag{9}$$

Lanning *et al.*[44] modified this model to obtain Eq. (10) and verified it against the experimental results of Carrol *et al.*[54] and Ronchi *et al.*[1] and also introduced the effect of gadolinia assuming a similar effect as observed for fresh fuels by Massih *et al.*[66]

The Duriez-modified NFI model (Eq. (11)) was proposed by Pacific Northwest National Laboratory (PNNL) for MOX fuels.[44] It is a combination of the fresh MOX fuel model of Duriez[14] and the modified NFI model (Eq. (10)) for irradiated UO_2, incorporating a modification of the high-temperature term of Duriez (C_{mod}). The constants $A(x)$, $B(x)$, and D are those proposed by Duriez for fresh MOX and x is the deviation from stoichiometry (i.e., $x = 2 - O/M$). This model was verified by PNNL using in-pile fuel central temperature measurements.

$$\lambda_{95} = \frac{1}{A + a \cdot gad + B \cdot T + f(bu) + (1 - 0.9e^{-0.04bu})g(bu)h(T)} + \frac{E}{T^2}e^{\frac{-F}{T}} \tag{10}$$

$$\lambda_{95} = \frac{1}{A(x) + B(x) \cdot T + f(bu) + (1 - 0.9e^{-0.04bu})g(bu)h(T)} + \frac{C_{mod}}{T^2}e^{\frac{-D}{T}} \tag{11}$$

2.06.6.4 Baron and NFIR (1998–2004)

Using NFIR experimental results for UO_2 up to a burnup of 80 MWd kg HM^{-1}, Baron[32] proposed a correlation in which thermal recovery during the out-of-pile annealing is accounted for by using the variation of the lattice parameter ξ (in Å) as a marker of the matrix damage evolution (Eq. (12) and **Table 3**). Comparison with experimental results shows good agreement, but the application of the correlation is possible only when the lattice parameter is known. For this reason, approximate formulae for A_0 and B_0 for the conductivity before recovery were deduced from the original plots: $A_0 = -3.422 \times 10^{-5}bu^2 + 7.792 \times 10^{-3}bu + 4.645 \times 10^{-2}$,

Table 3 Constants in the Baron model (Eq. (12)), the constant B_0 was modified using the plots in the original paper

$A_0 = 0.044819 + 0.005bu + 20(\xi - 5.4702)$ m K W^{-1}	$D = -4.302 \times 10^{10}$ W K m^{-1}
$B_0 = (2.12 - 0.0125bu - 70\ (\xi - 5.4702)) \times 10^{-4}$ m W^{-1}	$W = 1.41 \times 1.6 \times 10^{-19}$ J
$A_1 = 4$	$k = 1.38 \times 10^{-23}$ J K^{-1}
$A_2 = 0.611$	ξ lattice parameter in Å
$A_3 = 11.081$	*bu*: burnup in MWd t_U^{-1}
$B_1 = 0.8$	*Gd*: gadolinium weight content
$B_2 = 9.603 \times 10^{-4}$	*x*: absolute value of stoichiometric deviation
$B_3 = -1.768 \times 10^{-2}$	*q*: plutonium weight content
$C = 5.516 \times 10^9$	

Note: Baron, D., 1998. Fuel thermal conductivity: A review of the modeling available for UO_2, (U,Gd)O_2 and MOX fuel. In: Proceedings of the OECD/NEA Seminar on Thermal Performance of High Burn-up LWR Fuel, Cadarache, France.

Table 4 Constants of the thermal conductivity model described by Eq. (13) (SI units)

Parameter	*Value*	*Parameter*	*Value*
A_1	0.09592	B_1	0.00025
A_2	0.00614	B_2	0.00000181[a]
A_3	−0.000014	B_3	0.00000027[a]
A_4	0.0026	B_4	−0.01268763
A_5	0.1197	C	0.0132
A_6	0.01214167	D	0.00188
A_7	0.000540625	*Gd*	Gd weight content
A_8	−0.00005182292		

[a]Signs changed to correct the original values.

$B_0 = 1.328 \times 10^{-8}bu^2 - 2.292 \times 10^{-6}bu + 2.123 \times 10^{-4}$. The correlation includes the effect of Pu and Gd. The effects of these two additives were obtained from fresh fuel measurements and also from NFIR results for irradiated gadolinia fuel.[32]

$$K = \frac{1}{A_0 + A_1 \cdot x + A_2 \cdot g + A_3 \cdot g^2 + (B_0 \cdot (1 + B_1 \cdot q) + B_2 \cdot g + B_3 \cdot g^2)T_K} + \frac{C + D \cdot Gd}{T_K^2} e^{\frac{-W}{kT_K}} \tag{12}$$

An updated correlation for UO_2 and (U,Gd)O_2 (Eq. (13) and **Table 4**) was derived by Yagnik from the NFIR thermal conductivity results obtained on samples irradiated below 800°C.[67] This correlation takes into account the thermal recovery observed during laboratory measurements. The lattice thermal conductivity before and after thermal recovery is given by λ_{start} and λ_{end}, respectively, and the temperature dependence of the fission products redistribution and radiation damage recovery is given by the coefficient F. The burnup, *bu*, is in MWd kg HM^{-1} and T is in °C.

$$\lambda_{95}(Bu) = (1 - F) \cdot \lambda_{start} + F \cdot \lambda_{end} + \lambda_{el} \tag{13}$$

with

$$\lambda_{start} = \frac{1}{A_1 + A_2 \cdot Bu + A_3 \cdot Bu^2 + (B_1 - B_2 \cdot Bu) \cdot T(^\circ C)}$$

$$\lambda_{end} = \frac{1}{A_1 + A_4 \cdot Bu + (B_1 - B_3 \cdot Bu) \cdot T(^\circ C)}$$

$$\lambda_{el} = C \cdot e^{D \cdot T(^\circ C)}$$

$$F = 0.5\left(1 - \tan h\left(\frac{T(^\circ C) - 900}{150}\right)\right)$$

For (U,Gd)O_2 the same formula is used, replacing the coefficients A_1 and B_1 by:

$$A'(Gd) = \left(A_5 + A_6 \cdot Gd + A_7 \cdot Gd^2 + A_8 \cdot Gd^3\right) \cdot 0.26 \cdot e^{\frac{28.5875}{bu + 19.8085}} \qquad B'(Gd) = B_1 e^{B_4 \cdot Gd}$$

In this correlation, no information on the irradiation temperature or on the out-of-pile autoirradiation is explicitly taken into account. The temperature dependence of the coefficient F can be used to reconstruct experimental results obtained for different annealing temperatures (**Fig. 9**). Starting with an irradiated sample, F is calculated up to the first annealing temperature during the ascending temperature phase, and then kept constant during the descending phase. For the second annealing cycle, F is kept at the value used in the first cycle up to the first annealing temperature, and then F is recalculated when this temperature is exceeded. Then, for the evaluation during the descending temperature phase, F is kept at the value corresponding to the highest temperature reached in the second cycle. According to Eq. (13), most of the out-of-pile recovery takes place in the range from 900 to 1500K.

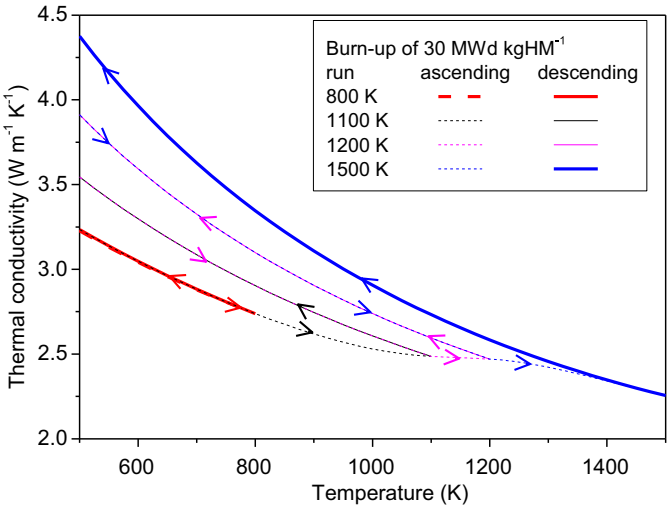

Fig. 9 Thermal conductivity during out-of-pile annealing cycles as predicted by the Nuclear Fuel Industry Research correlation for a burnup of 30 MWd kg HM^{-1}.

Table 5 Parameters of the thermal conductivity model of Kitajima *et al.*

$T < 1273$K		$T > 1473$K	$1273 \leq T \leq 1473$K; linear interpolation between the conductivities in the two temperature regions
$A = 40 + 4.12bu$		$A = 40 + 1.74bu$	
$bu < 50$	$B = 0.22$	$B = 0.22 + 0.0003bu$	
$50 < bu < 80$	$B = 0.447 - 0.00453bu$		
$80 < bu$	$B = 0.084$		

Source: Kinoshita, M., Sonoda, T., Kitajima, S., *et al.*, 2004. High burnup rim project (III): Properties of rim-structured fuel. In: Proceedings of the 2004 ANS International Meetingon LWR Fuel Performance, p. 207. Orlando, FL.

This temperature range for recovery appears to be relatively high and may be related to the irradiation temperature of the samples, which is specified only as being below 800°C.

2.06.6.5 HBRP (2004)

UO_2 and (U,Gd)O_2 samples were irradiated in the framework of the HBRP which comprised a matrix of four burnups and four irradiation temperatures.[63] The samples were in the form of 1-mm-thick disks, irradiated at constant, controlled temperature (~750–1500K) and up to different burnups in the range from 34 to 96 MWd kg HM^{-1}.[65]

Kinoshita *et al.*[63] derived a first correlation (Eq. (14)) summarizing the HBRP thermal conductivity results and including the effect of the HBS structure formation (**Table 5**). A slight increase of the conductivity normalized to 100% TD was observed after its formation, attributed to the matrix damage recovery and to the transfer of the gas atoms to the pores.

$$\lambda = \frac{1}{A + B \cdot T} + \lambda_e \tag{14}$$

where λ_e is the electronic contribution to the conductivity.

Ronchi obtained a second model based on the HBRP results.[1] Three temperatures are taken into account: the irradiation temperature, T_{irr}, which summarizes the state of the fuel at EOL; the out-of-pile annealing temperature, T_{ann}, which indicates how much damage was recovered; and the temperature, T, at which the thermal conductivity is measured. The thermal diffusivity was measured during annealing cycles with maximum temperatures lower and higher than the irradiation temperatures when the samples did not fragment.

The phonon thermal conductivity (normalized to 5 vol% porosity) is expressed by

$$\lambda = (A(T_{irr}, T_{ann}, bu) + B(T_{irr}, T_{ann}, bu)T)^{-1} \tag{15}$$

where T is the instant application temperature (300–1500K); T_{irr} is the irradiation temperature (700–1450K); T_{ann} is the maximum temperature (700–1450K) reached during out-of-pile annealing; and bu is the local fuel burnup, in MWd kg HM^{-1} (up to 100).

The different contributions to the degradation of the thermal conductivity were quantified. The coefficient A, as given by Eq. (16), is the sum of the fresh fuel value, 0.046 m K W^{-1}; the contribution of nonvolatile and volatile fission products,

$\Gamma(bu, \text{GIS})$ (GIS is the fraction of gaseous and volatile fission products present as dispersed atoms in the fuel matrix); the autoirradiation damage, $\delta A_{\text{Auto}}(T_m, bu)$; and the in-pile radiation damage, $\delta A_{\text{EOL}}(T_m, bu)$.

$$A(T_{irr}, T_{ann}, bu) = 0.046 + \Gamma(bu, GIS) + \delta A_{\text{Auto}}(T_m, bu) + \delta A_{\text{EOL}}(T_m, bu) \tag{16}$$

The temperature $T_m = \max(T_{irr}, T_{ann})$ takes into account the irreversible recovery taking place when the irradiation temperature is exceeded. The damage state of the fuel corresponds to that at EOL as determined from T_{irr}, but as soon as T_{irr} is exceeded during the measurement, the damage state is determined by T_{ann}.

The effect of autoirradiation damage produced between EOL and the time of the measurements is determined by measuring the recovery during measurements up to the irradiation temperature. This autoirradiation effect was found to be present in all samples, independently of the irradiation temperature and burnup. This means that the values of A at EOL were always lower than those measured in laboratory. A compensation was applied, but it is not discussed here.[1] The effect of parameters that are not sensitive to temperature was assessed from the results obtained after laboratory annealing. These are the soluble fission products (whose effect was analyzed with the phonon scattering formulae based on the evaluation of the phonon scattering cross section Γ) and the nonvolatile fission products (metallic and ceramic precipitates, the effect of which was analyzed by using the theory of the effective conductivity of composite materials). The effect of these parameters on the coefficients A and B was found to be proportional to the burnup and therefore could not be discerned from the experimental results. This effect was integrated in the parameter Γ as a linear burnup effect (Eq. (17)). Gaseous and volatile fission products trapped at the atomic state in the fuel matrix also contribute to the phonon scattering, and their effect is therefore included in the phonon scattering cross section Γ. Its maximum amplitude was deduced by analyzing the evolution of the conductivity due to the HBS formation. The temperature and microstructure dependence were interpreted by determining the thermodynamic state of the fission gas, calculated with a diffusion/precipitation/release model[18] predicting the fraction of gas dynamically dissolved (gas in solid (GIS)) and precipitated (gas in bubbles). The latter state was found to depend both on temperature and grain size, and this last parameter accounts for the effect of rim restructuring. This effect was integrated in the parameter Γ, which depends on bu and GIS as shown in Eq. (17).

$$\Gamma(bu, GIS) = 9.02 \cdot 10^{-4} \cdot bu \cdot GIS + 1.74 \cdot 10^{-3} \cdot bu + 7.51 \cdot 10^{-3} \tag{17}$$

An approximate expression of GIS needed for evaluating Eq. (17) is given by Eq. (18). The numerator takes into account the irradiation temperature and the burnup, which are indicators for HBS formation, taking into account the precipitation of a fraction of the fission gas inventory at that transition. The denominator represents the formation of gas bubbles and fission product inclusions that takes place at high irradiation or annealing temperatures, independently of the microstructure.

$$\text{GIS}(bu, T_{irr}, T_{ann}) = \frac{1 - 0.9\left[1 + \exp\left(\frac{T_{irr} - 950}{30}\right)\right]^{-1}\left[1 + \exp\left(\frac{73 - bu}{2}\right)\right]^{-1}}{\left[1 + \exp\left(\frac{T_{irr} - 1350}{200}\right)\right]\left[1 + \exp\left(\frac{T_{ann} - 1350}{200}\right)\right]} \tag{18}$$

The contribution of in-pile radiation damage to the thermal conductivity deterioration was quantified from the measured magnitude and temperature dependence of the recovery for measurement temperatures higher than T_{irr}. The in-pile radiation damage could be investigated in samples that did not fragment. These generally are characterized by low burnup and low irradiation temperatures. After subtracting the out-of-pile autoirradiation effect, a conductivity recovery in the form of a decrease of the coefficient A was observed. No significant recovery was observed below 800K. The recovery took place in two stages: between 800 and 1000K and between 1200 and 1350K. The variation of A due to the change in the effective concentration of irradiation defects at EOL, δA_{EOL}, was found to be proportional to burnup and can be expressed by Eq. (19), with $T_m = \max(T_{irr}, T_{ann})$.

$$\delta A_{\text{EOL}}(T_m, bu) = \frac{bu}{850}\left[\left(1 + \exp\left(\frac{T_m - 950}{25}\right)\right)^{-1} + \left(1 + \exp\left(\frac{T_m - 1300}{35}\right)\right)^{-1} - 0.0525\right] (\text{m K W}^{-1}) \tag{19}$$

In agreement with the experimental results, the effect of in-pile and out-of-pile thermal annealing of irradiation defects for a given temperature is equivalent in Eq. (19), so that $\delta A_{\text{EOL}}(T_{irr}, bu)$ is calculated by the same function, replacing T_{irr} by T_{ann} when $T_{ann} > T_{irr}$.

The variation of the coefficient B was analyzed using the same methodology and is described by very similar equations but is not presented here.

The thermal conductivity of UO_2 at EOL as a function of burnup for different irradiation temperatures (obtained with $T = T_{irr} = T_{ann}$) is shown in **Fig. 10**. In this model, the formation of the HBS induces a large decrease in the fission gas concentration dissolved in the matrix and has a positive effect on the lattice thermal conductivity (i.e., normalized to 5 vol% porosity) as seen for the curves for irradiation temperatures of 300, 600, and 900K in **Fig. 10**. If not corrected for porosity differences, the fuel thermal conductivity decreases with burnup increase, even during HBS formation because of the concomitant increase in porosity. When the burnup further increases, the degradation continues, as a result of the accumulation of fission products. A similar model was obtained for $(U,Gd)O_2$,[64] adapting the constants of the model for UO_2 in order to take into account the difference between unirradiated UO_2 and $(U,Gd)O_2$.

2.06.6.6 A Correlation for UO_2 and MOX

Systematic studies of unirradiated MOX fuel[14] have shown that the thermal conductivity is significantly lower than that of UO_2 and that the effects of the Pu concentration (in the range 3–15 wt%) and microstructure were insignificant. Investigations were performed by comparing the experimental results available for irradiated UO_2 and MOX fuels with different microstructures and

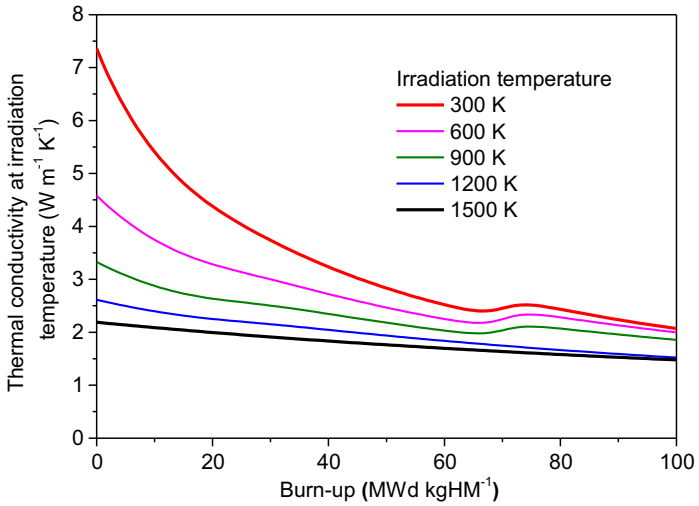

Fig. 10 Thermal conductivity of UO_2 as a function of burn-up for different irradiation temperatures according to the model of Ronchi *et al.*,[1] evaluated at the irradiation temperature (at end of life and for 95% TD).

burnups in the range 0.4–100 MWd kg HM^{-1}.[1,25,38,59,61] A model for the comparison between fuels with different burnups and irradiation conditions is required. Starting from the Ronchi model for UO_2,[1] a simplified version was derived for purposes of comparison. The parameters that have to be included in such a correlation are the burnup and irradiation temperature. The irradiation temperature is required to describe the increase in thermal conductivity observed when moving from the periphery to the pellet center, in regions with almost constant burnup.[25] The only measurements that are to be considered are those obtained after annealing at the irradiation temperature and measured during the descending temperature phase. The measurements obtained during the ascending temperature phase up to the irradiation temperature were not considered because annealing takes place progressively during such a measurement run. The out-of-pile damage, due to autoirradiation, is assumed to be annealed at this temperature. In order to investigate the differences or similarities between irradiated UO_2 and MOX, the correlation was fitted to three different datasets: UO_2 alone, MOX alone, and UO_2 and MOX together.

As a preliminary approach, a formula including the effect of the burnup only is investigated: $\lambda = 1/(A+BT)$ with A and B depending linearly on burnup: $A = A_1 + A_2 bu$ and $B = B_1 + B_2 bu$ (where bu is the burnup in MWd kg HM^{-1}). As the formula is validated only for measurements up to 1500K, no high-temperature contribution is introduced. The extrapolation to zero burnup has to be considered carefully when such a simple formula is used, because of the rapid degradation in thermal conductivity occurring at very low burnups, linked to the buildup of radiation damage. Preliminary tests have shown that the parameters A_1 and B_1 cannot have the values corresponding to fresh fuel. This is well demonstrated by the experimental results obtained for UO_2 fuel with the very low burnup of 0.4 MWd kg HM^{-1}[38]: the degradation of the thermal conductivity at this burnup is much higher than that predicted by a formula valid up to 100 MWd kg HM^{-1}. The extrapolation to zero burnup requires introducing a supplementary term in the correlation. The 0.4 MWd kg HM^{-1} sample was not used because a simple burn-up dependence could not predict a sudden conductivity drop at the beginning of irradiation, and the next lowest burnup sample has a burnup of 23 MWd kg HM^{-1}. The four free parameters A_1, A_2, B_1, and B_2 were evaluated by a least-squares method and it was shown that it is not justified to propose distinct correlations for UO_2 and MOX. The obtained correlation corresponds to the following values of the parameters:

$$A_1 = 0.11906 \text{ m K W}^{-1}; \quad A_2 = 0.002617 \text{ m K W}^{-1}$$

$$B_1 = 2.5974 \cdot 10^{-4} \text{ m W}^{-1}; \quad B_2 = -8.726 \cdot 10^{-7} \text{ m W}^{-1}.$$

As both samples with low and high irradiation temperatures were considered in this study, the results given by such a correlation cannot provide an optimum prediction for each particular sample. In a second correlation, the irradiation temperature dependence was introduced using a formula already proposed,[1] based on a two-step annealing of radiation damage in the temperature range 500–1500K: the first at 950K and the second at 1300K. The thermal conductivity (normalized to 5% porosity) is expressed (Eq. (20)) as $\lambda = (A(bu, T_{irr}) + B(bu, T_{irr})T)^{-1}$, where T is the measurement temperature (300–1500K), T_{irr} is the irradiation temperature (600–1500K), and bu is the burnup (23–100 MWd kg HM^{-1}).

$$A(bu, T_{irr}) = A_1 + A_2 bu + A_3 bu\, f(T_{irr}) \text{ and } B(bu, T_{irr}) = B_1 + B_2 bu + B_3 bu\, f(T_{irr}) \tag{20}$$

with

$$f(T_{irr}) = \left(1 + \exp\left(\frac{T_{irr} - 950}{25}\right)\right)^{-1} + \left(1 + \exp\left(\frac{T_{irr} - 1300}{35}\right)\right)^{-1}$$

The results of the parameter estimation process show that the average interpolation error for UO_2 and MOX fuels is lower than in the previous case, but all the qualitative observations remain valid. It is confirmed that it is not justified to propose separate correlations for the UO_2 and MOX fuels. The correlation is defined by (in SI units):

$$A_1 = 0.1088; \quad A_2 = 1.664 \cdot 10^{-3}; \quad A_3 = 8.371 \cdot 10^{-4}$$

$$B_1 = 2.932 \cdot 10^{-4}; \quad B_2 = -5.548 \cdot 10^{-7}; \quad B_3 = -7.189 \cdot 10^{-6}$$

The interpolation error was therefore reduced by introducing the irradiation temperature as a parameter in the correlation, and the predictions for samples with high irradiation temperatures were particularly improved. The interpolation error might be reduced further by introducing supplementary parameters, such as the presence of the HBS structure. However, if the uncertainties in the experimental thermal conductivities are taken into account (about 10% for irradiated fuel), the average error of 7.4% obtained with the present correlation is already acceptable.

2.06.7 Comparison of the Results Obtained Using Different Models

The available models range from correlations built from in-pile or out-of-pile measurements to combinations of models or results. The thermal conductivity predictions at 95% TD for UO_2 obtained with the three approaches presented in this article are compared for the burnups of 30 (Fig. 11) and 80 (Fig. 12) MWd kg HM^{-1} in the temperature range from 500 to 1500K. The model of Lucuta[39] was obtained from measurements on simulated irradiated fuels, and the model of the Halden Reactor Project[45] was derived from in-pile central temperature data. The models published from out-of-pile measurements by NFI (Ohira and Itagaki[55] and Lanning *et al.*[44]), by NFIR (Baron[32] and Yagnik *et al.*[67]), by HBRP (Ronchi *et al.*[1]), and by the correlation for UO_2 and MOX accounting for differences in irradiation temperature (Eq. (20)) were selected. The calculations were done at the irradiation temperature, that is, without taking into account out-of-pile recovery during annealing at higher temperatures. For the models considering only one temperature, that is, the measurement temperature, it was assumed to be equivalent to the irradiation temperature.

The model of Lucuta predicts the weakest degradation with burnup compared with both out-of-pile and in-pile measurements; this degradation is considered too low by Ohira and Itagaki[55] and Lanning *et al.*[44] This model is therefore not considered in the following discussion. However, Minato *et al.*[57] found that this model was in good agreement with their experimental results.

The model of the Halden Reactor Project and the models obtained from out-of-pile measurements give predictions that are in the same range. Some scatter exists, due to the differences in the nature and number of samples used: no model was produced using samples covering the entire burnup and irradiation temperature range considered. At the burnup of 30 MWd kg HM^{-1} (Fig. 11), the scatter is moderate at low temperatures and increases with temperature. This increase reflects the reduced number of samples available for high irradiation temperatures. To our knowledge, only the correlations of Ronchi and "UO_2 and MOX" consider samples with irradiation temperature up to 1500K and these correlations give the lowest predictions at high temperatures. At the burnup of 80 MWd kg HM^{-1} (Fig. 12), the scatter between the different models is of about 20%, independent of the temperature. The model of Ronchi shows the positive effect of HBS formation: it predicts the highest values for low irradiation temperatures. For both burnup values, it is noteworthy that even correlations obtained from almost similar experimental results do not give identical predictions as a result of the different approaches and aims of the authors. Differences exist in the analysis of the out-of-pile annealing cycles (i.e., the selection of the data used from the large number of data produced by such cycles), taking

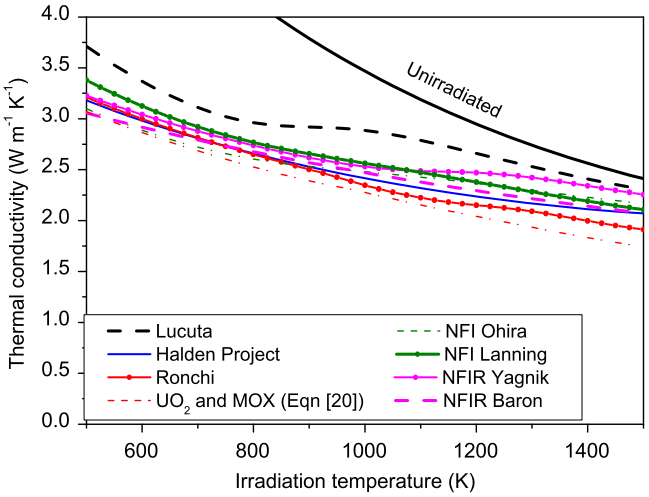

Fig. 11 Thermal conductivity at 95% TD as a function of temperature at a burnup of 30 MWd kg HM^{-1} according to different models.

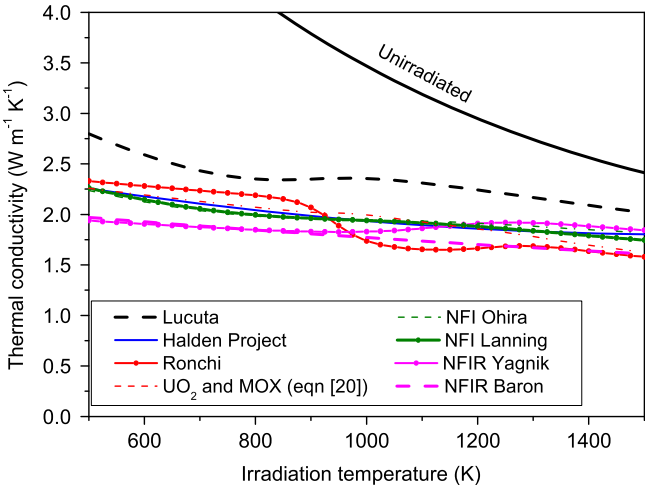

Fig. 12 Thermal conductivity at 95% TD as a function of temperature at a burnup of 80 MWd kg HM^{-1} according to different models.

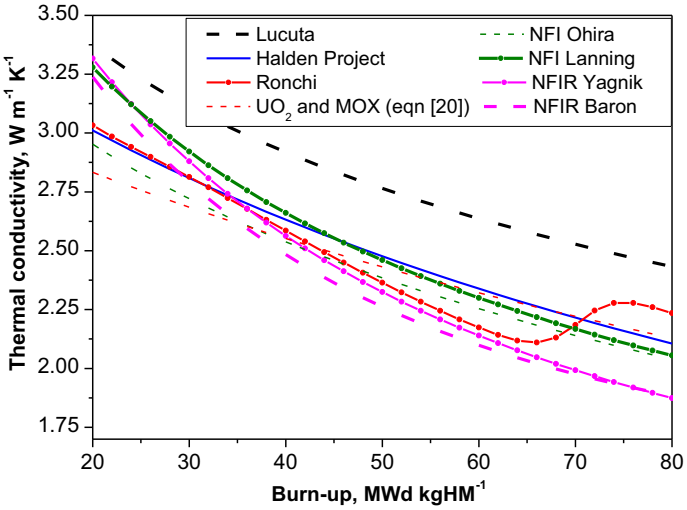

Fig. 13 Thermal conductivity at 95% TD as a function of burnup at an irradiation temperature of 700K according to different models.

into account or not the irradiation temperature and in the mathematical form adopted, which reflects the phenomena included such as the HBS formation or the out-of-pile annealing behavior.

The thermal conductivity as a function of burnup for an irradiation temperature of 700K is plotted in **Fig. 13**. It can be seen that the scatter is high at low and high burnup. At low burnup, this is explained by the lack of samples and the fact that a simple formula valid at intermediate and high burnups cannot be extrapolated to zero burnup, where the degradation of the thermal conductivity is much faster. At high burnup, the scatter is due to the reduced number of samples and the fragmentation of the samples that complicates the measurements.

The thermal conductivities of (U,Gd)O_2 and MOX fuels follow the same trend as UO_2 in terms of burnup degradation. The main difference between the models is how the ratio between the conductivity of the fuel with an additive and UO_2 changes with burnup. For MOX fuel, the ratios obtained with the models of Lanning (Duriez-NFI[44]), Baron,[32] "UO_2 and MOX" (Eq. (20)), and the Halden Project[45] are shown in **Fig. 14**. Only the Halden Project formula and the "UO_2 and MOX" correlations are based on experiments; the Lanning and Baron correlations are derived from measurements on unirradiated fuel. The "UO_2 and MOX" correlation predicts a ratio of 1 for burnups higher than 32 MWd kg HM^{-1}, as observed in out-of-pile measurements.

The ratio is larger for the (U,Gd)O_2 fuels but is also predicted to decrease with burnup, as illustrated in **Fig. 14** with the models of Baron,[32] NFI modified by Lanning *et al.*,[44] and NFIR.[67] This trend was confirmed by the HBRP results,[64] which also showed that even at high burn-up, the difference in thermal conductivity between (U, Gd)O_2 and UO_2 remains significant. Therefore, both for (U,Gd)O_2 and MOX fuels, as well as for the Cr-doped fuel,[26] the degradation observed for the fresh fuels as compared with standard UO_2 decreases with burnup.

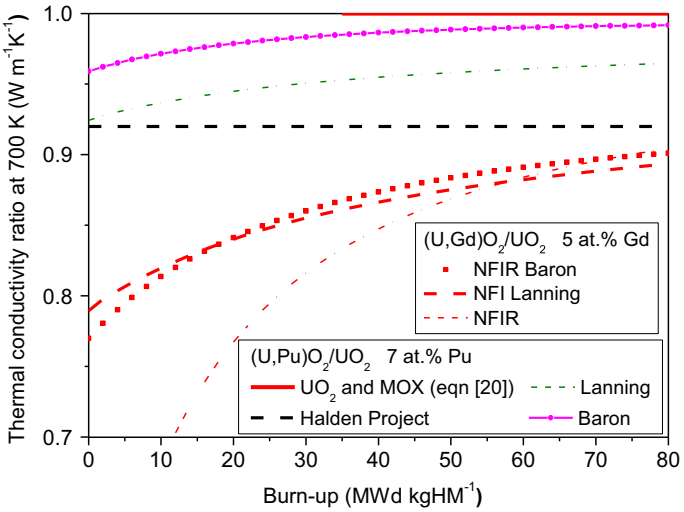

Fig. 14 Ratio of the conductivities of the $(U,Gd)O_2$ and mixed oxide fuels to that of UO_2 as a function of burnup.

2.06.8 Melting Behavior

The melting temperature (liquidus) of unirradiated UO_2 fuel depends on its stoichiometry, while for MOX fuel it also depends on the plutonium and minor actinides (mainly americium) contents.

When the fuel is irradiated, the melting behavior still depends on these parameters and the liquidus temperature is expected to slowly decrease with burn-up.

Experimental efforts for irradiated fuels have mainly concentrated on FBR MOX, because of the very high operation temperature of these fuels, close to the melting point at pellet center already under normal irradiation conditions. Because of the very high temperatures of interest, experiments are delicate, already for unirradiated fuel. Due to these difficulties, and also to the lack of irradiated samples covering a wide range of Pu and Am contents or stoichiometry, the effect of these parameters is investigated with fresh fuel samples.

The effect of the plutonium content on the fresh MOX fuels melting temperature was recently updated[68,69] thanks to a new experimental method based on laser heating and melting of a circular spot of approximately 2–3 mm in diameter on the surface of the sample, not requiring a containment material for the molten material. Due to the fast heating and cooling rates, a clear distinction between solidus and liquidus can not always be made but a narrow melting/freezing temperature range can be defined. UO_2-rich samples were heated under an inert atmosphere (argon), whereas PuO_2-rich ones were heated under dry air (0.3 MPa), in order to minimise oxygen losses from the condensed phases. Eq. (21) was obtained on the basis of these results and describes the experimental results well, taking into account the uncertainties ($\pm$35K), except for the melting temperature obtained for 75% Pu, which was measured significantly lower. The complexity of the melting behavior and of the effect of the measurement atmosphere on the samples stoichiometry requires modeling work and these results were integrated in the CALPHAD model which can be used to obtain the solidus and liquidus.

Older data were usually determined by a thermal arrest method using a tungsten capsule, but a reaction between the sample and the tungsten containment was observed (particularly for MOX samples containing more than 20% Pu[70]) which led to an underestimation of the solidus temperature as illustrated by the recommendation of Carbajo[71] in **Fig. 15**. The thermal arrest method was improved by Kato[70] using a liner in the tungsten capsule to avoid the reaction with the sample, these new results are shown in **Fig. 15** and agree generally well with Eq. (21).

The effect of burn-up was reviewed by Carbajo in 2001[71] for UO_2, LWR and FBR MOX, and a decrease of 0.5K for each MWd $kgHM^{-1}$ burn-up was recommended, based on experimental data up to the burn-up of 100 MWd kg HM^{-1}. The experimental result of Hirosawa[72], showing a decrease of 0.6K each MWd kg HM^{-1}, agree well with this recommendation. In the same review but without providing supporting information, Carbajo states that the melting point should decrease with the deviation from stoichiometry. Such behavior was observed for the effect of hyperstoichiometry in fresh UO_2[73] but in MOX fuel an increase in solidus temperature with increasing hypostoichiometry was observed by Kato[74]: for MOX with 20% Pu the increase between the stoichiometry of 2.00 and 1.94 was measured to be of about 30K. A similar trend was predicted by Guéneau using thermodynamic modeling[75]. A previous study by Konno[76] showed a decrease of the solidus temperature with increasing hypostoichiometry in MOX with 20% Pu, and the opposite behavior in MOX with 40% Pu.

Because of the oxygen redistribution observed during irradiation of FBR fuels, the stoichiometry effect is an important parameter for the determination of the margin to melt, and it is recognised that supplementary experimental investigations are needed.

Concerning the effect on the americium content on the melting point, experimental investigations by Kato[73] have shown a decrease of 4K per 1% Am content. In a previous thermodynamic study by Konno[77] a decrease of 10K per 1% Am

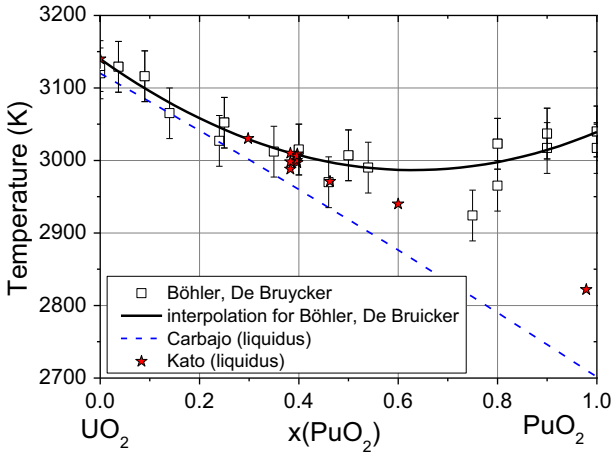

Fig. 15 Melting temperature of $(U,Pu)O_2$ as a function of the Pu content.[68–71] The interpolation corresponds to Eq. (21).

content in MOX with 20% Pu was predicted. For the low Am contents relevant for the MOX fuels, this effect is therefore relatively small.

$$T_M = 385x^2 - 486x + 3140 \tag{21}$$

where T_M is the melting temperature in K and x is the Pu atomic fraction

The melting point (liquidus) of unirradiated Gd-doped UO_2 fuel was measured by Kang[78] for Gd_2O_3 contents of 4, 6, 8 and 12 wt% using a thermal arrest method with a tungsten capsule. Compared to pure UO_2, the liquidus temperature was found to decrease with the Gd_2O_3 content, with a decrease of about 120K at 12 wt% Gd_2O_3. The same trend was also observed by Beals[79].

Using the same technique, Yamanouchi[80] measured the solidus temperature of fresh and irradiated Gd-doped UO_2 with a Gd_2O_3 content of 2 wt%. Compared to fresh UO_2, no decrease in solidus temperature was observed, neither in the unirradiated Gd-doped fuel, nor in the Gd-doped fuel irradiated at 15 and 29 MWd kg HM^{-1}.

2.06.9 Conclusions

UO_2 is the most studied nuclear fuel, with characterization results accumulated since more than 50 years. Investigations are also conducted to assess the high burnup effects and the impact of additives such as Pu, Gd, and Cr. Experimental and theoretical studies of the influence of microstructure on the thermal conductivity of fresh and irradiated MOX fuels are conducted using UO_2 as a reference. The addition of a few percent of Pu in UO_2 lowers the thermal conductivity of the fresh fuel but does not significantly influence the thermal conductivity at intermediate and high burnups. Recent studies have also shown that the effect of the MOX microstructure is negligible. As a result, a common correlation was proposed for irradiated UO_2 and MOX.[61] Further studies will be needed, linked to the increase of the discharge burnup, made possible by increase of the enrichment of UO_2 fuel and of the plutonium content of MOX fuel. For MOX fuel, the Pu content in fresh fuel will further be increased because of the degradation of the isotopic composition of the Pu obtained from reprocessing of spent high-burnup UO_2. Other developments are necessary, aimed at improving the precision and validity domain of the correlations: extrapolation down to zero burnup, effect of the HBS, and in-pile and out-of-pile annealing of the radiation damage due to temperature variations.

The choice of an appropriate correlation or approach depends on the needs, between the simple formulae describing only the average expected degradation with burnup or more complex formulae adapted to precise studies taking into account irradiation conditions (average irradiation temperature at EOL or irradiation temperature history).

Because of the nature of irradiated fuel, the precision that can be reached for the thermal conductivity is limited, and fluctuations linked to the uncertainties on the irradiation conditions will remain. Only a complete integration of the irradiation history in the model can lead to a perfect prediction, assuming that the effect of each parameter can be quantified, which is not the case currently. High-temperature data are almost nonexistent because of the brittleness of the samples: in particular, high-burnup fuel samples irradiated under normal conditions are hardly resistant to out-of-pile annealing at temperatures higher than about the irradiation temperature. The prediction of the thermal conductivity at very high temperatures ($T > 1500$K) is therefore not straightforward.

Purely theoretical studies are not found in the literature because of the complex structure and composition of irradiated fuel, and only semiempirical studies are possible at present: the mathematical formulation is chosen from theoretical considerations and the coefficients are fitted to experimental results. Theoretical studies exist only for single effects, such as the porosity and pore shape[6] or the effect of the microstructure of MOX fuels.[48]

The melting point of irradiated fuel was shown to depend relatively weakly on burn-up, but experimental difficulties linked to the high temperatures of interest and to the reaction of the molten samples with the capsules have led in the past to too

conservative recommendations for fresh MOX fuels with high Pu contents. The quantification of the effect of non-stoichiometry on the melting point requires further investigations, already for fresh MOX fuels.

See also: 2.05 Radiation Effects in UO_2. 7.03 Thermodynamic and Thermophysical Properties of the Actinide Oxides

References

1. Ronchi, C., Sheindlin, M., Staicu, D., Kinoshita, M., 2004. J. Nucl. Mater. 327, 58.
2. Quintard, M., Whitaker, S., 1993. Chem. Eng. Sci. 48, 2537–2564.
3. Suzuki, M., Saitou, H., 2006. Light Water Reactor Fuel Analysis Code FEMAXI-6 (Ver.1). Report JAEA-Data/Code 2005-003. JAEA.
4. Maxwell, J.C., 1954. A Treatise on Electricity and Magnetism, third ed. Dover, NY: Clarendon Press, pp. 435–441.
5. Loeb, A.L., 1954. J. Am. Ceram. Soc. 37, 96.
6. Bakker, K., Konings, R.J.M., 1996. Nucl. Technol. 115, 91–99.
7. Fink, J.K., 2000. J. Nucl. Mater. 279, 1.
8. Lucuta, P.G., Matzke, H.J., Verall, R.A., 1994. J. Nucl. Mater. 217, 279–286.
9. Eucken, A., 1932. Forsch Gebiete Ingenieur B-3. pp. 6–21.
10. Ambegaoker, Y., 1966. Trans. Am. Nucl. Soc. 9, 488.
11. Leibfried, G., Schlömann, E., 1954. Nachr. Akad. Wiss. Göttingen. Math. Phys. KI 2-A. 71–93.
12. Kleykamp, H., 1985. J. Nucl. Mater. 131, 221–246.
13. Abeles, B., 1963. Phys. Rev. 131, 507.
14. Duriez, C., Alessandri, J.P., Gervais, T., Philipponneau, Y., 2000. J. Nucl. Mater. 277, 143.
15. Ishimoto, S., Hirai, M., Ito, K., Korei, Y., 1994. J. Nucl. Sci. Technol. 31, 796.
16. Fukushima, S., Ohmichi, T., Maeda, A., Hanada, M., 1983. J. Nucl. Mater. 116, 287–296.
17. Murti, P.S., Mathews, C.K., 1990. High Temp. High Press. 22, 379–390.
18. Syros, C., Sakellaridis, J., Ronchi, C., 1989. J. Nucl. Mater. 168, 65–69.
19. Martin, D.G., 1982. J. Nucl. Mater. 110, 73–94.
20. Une, K., *et al.*, 1991. J. Nucl. Sci. Technol. 28, 409.
21. Matzke, H.J., 1994. J. Nucl. Mater. 208, 18.
22. Spino, J., Peerani, P., 2008. J. Nucl. Mater. 375, 8–25.
23. Sonoda, T., Kameyama, T., Sasahara, A. *et al.*, 2007. Clarification of rim structure effects on properties and behaviour of LWR UO_2 fuels and gadolinia doped fuels. In: Proceedings of the 2007 International LWR Fuel Performance Meeting, San Francisco, Paper 1026. September 30–October 3, 2007. CA.
24. Fujii, H., Teshima, H., Kanasugi, K., Sendo, T., 2006. J. Nucl. Sci. Technol. 43, 998.
25. Cozzo, C., Staicu, D., Pagliosa, G., *et al.*, 2010. J. Nucl. Mater. 400, 213–217.
26. Caillot, L., Noirot, J., Pontillon, Y., Valin, S., 2006. TANOXOS: An analytical irradiation program aiming at understanding the behaviour of various doped UO_2 fuels. In: Proceedings of the 2006 International LWR Fuel Performance Meeting, October 22–26, 2006. Salamanca, Spain.
27. Staicu, D., Cozzo, C., Papaioannou, D., Konings, R.J.M., Walker, C.T., 2009. Thermal conductivity of fresh and irradiated MOX fuel: Influence of microstructure. In: Proceedings of the Top Fuel 2009, Paper 2107. September 6–10, 2009. Paris, France.
28. Staicu, D., Baron, D., 2010. Discussion about the main parameters affecting the thermal conductivity of LWR UO_2 and MOX fuels. In: Proceedings of the International Meeting on LWR Fuel Performance, September 26–29, 2010. Orlando, FL.
29. Brandt, R., Neuer, G., 1976. J. Non-Equilib. Thermodyn. 1, 3.
30. Spino, J., Vennix, K., Coquerelle, M., 1996. J. Nucl. Mater. 231, 179–190.
31. Walker, C.T., 1999. J. Nucl. Mater. 275, 56–62.
32. Baron, D., 1998. Fuel thermal conductivity: A review of the modeling available for UO_2, $(U,Gd)O_2$ and MOX fuel. In: Proceedings of the OECD/NEA Seminar on Thermal Performance of High Burn-up LWR Fuel, Cadarache, France.
33. Verall, R.A., Lucuta, P.G., 1996. J. Nucl. Mater. 228, 251.
34. Matsui, T., Arita, Y., Naito, K., 1992. J. Nucl. Mater. 188, 205.
35. Takahashi, Y., Asou, M., 1993. J. Nucl. Mater. 201, 108.
36. Gomme, R.A., Carrol, J.C., Shaw, T.L., 1998. High Temp. High Press. 30, 135–140.
37. Yagnik, S., Turnbull, J.A., 2006. Specific heat and density of high burnup fuel. In: Proceedings of the 2006 International LWR Fuel Performance Meeting, October 22–26, 2006. Salamanca, Spain.
38. Staicu, D., Wiss, T., Rondinella, V.V., *et al.*, 2010. J. Nucl. Mater. 397, 8–18.
39. Lucuta, P.G., Matzke, H., Hastings, I.J., 1996. J. Nucl. Mater. 232, 166.
40. Kang, K.H., Moon, H.S., Song, K.C., *et al.*, 2007. Int. J. Thermophys. 28, 1595–1606.
41. Hartlib, S.M., Hough, A., Waite, M.P., Hall, A.R., 1973. Hanoell Report AERE-R 7325.
42. Philipponneau, Y., 1992. J. Nucl. Mater. 188, 194–197.
43. Lanning, D.D., Beyer, C.E., Painter, C.L., 1997. FRAPCON-3: Modifications to Fuel Rod Material Properties and Performance Models for High Burn-Up Application, NUREG/CR-6534.
44. Lanning, D.D., Beyer, C.E., Geelhood, K.J., 2005. Report NUREG/CR-6534, vol. 4, PNNL-11513.
45. Wiesenack, W., 1997. Assessment of UO_2 conductivity degradation based on in-pile temperature data. In: Proceedings of ANS International Meeting on LWR Fuel Performance, p. 507. Portland, OR.
46. Lee, B.H., Koo, Y.H., Sohn, D.S., 2001. J. Nucl. Sci. Technol. 38, 45–52.
47. Kampf, H., Karsten, G., 1970. J. Nucl. Technol. 9, 228.
48. Wiesenack, W., Lee, B.H., Sohn, D.S., 2005. Nucl. Eng. Technol. 37, 317–326.
49. Nakae, N., Akiyama, H., Miura, H., *et al.*, 2013. J. Nucl. Mater. 440, 515–523.
50. Bernard, L.C., Jacoud, J.L., Vesco, P., 2002. J. Nucl. Mater. 302, 125–134.
51. Hirai, M., Amaya, M., Wakashima, Y. *et al.*, 1996. Thermal diffusivity measurements of irradiated UO_2 pellets. In: Proceedings of the IAEA TCM on Advances in Pellet Technology for Improved Performance at High Burn-up, IAEA-TECDOC-1036. October 26–November 1, 1996. Tokyo, Japan.
52. Sheindlin, M., Halton, D., Musella, M., Ronchi, C., 1998. Rev. Sci. Instrum. 69, 1426.

53. Beyer, C.E., Lanning, D.D., 1998. Review of fuel thermal conductivity data and models. In: Proceedings of the OECD/NEA Seminar on Thermal Performance of High Burn-up LWR Fuel, Cadarache, France.
54. Carrol, J., Gomme, R., Leech, N.A., 1994. Thermal diffusivity measurements on unirradiated archive fuel, and fuel irradiated in the Halden IFA-558 experiment. In: Proceedings of the Enlarged Halden Programme Meeting, October 30–November 4, 1994. Bolkesjo, Norway.
55. Ohira, K., Itagaki, N., 1997. Thermal conductivity measurements of high burnup UO_2 pellet and a benchmark calculation of fuel center temperature. In: Proceedings of the ANS International Meeting on LWR Fuel Performance, March 2–6, 1997. p. 541. Portland, OR.
56. Nakamura, J., 1998. Thermal diffusivity of high burn-up UO_2 pellet irradiated at HBWR. In Thermal Performance of High Burn-Up LWR Fuel. Cadarache, France: OECD.
57. Minato, K., Shiratori, T., Serizawa, H., *et al*., 2001. J. Nucl. Mater. 288, 57–65.
58. Amaya, M., Hirai, M., Sakurai, H., *et al*., 2002. J. Nucl. Mater. 300, 57.
59. Walker, C.T., Staicu, D., Sheindlin, M., *et al*., 2006. J. Nucl. Mater. 350, 19–39.
60. Yamamoto, K., Hirosawa, T., Yoshikawa, K., Morozumi, K., Nomura, S., 1993. J. Nucl. Mater. 204, 85–92.
61. Staicu, D., Cozzo, C., Pagliosa, G., *et al*., 2011. J. Nucl. Mater. 412, 129–137.
62. Yagnik, S., 2000. Thermal conductivity recovery phenomenon in irradiated UO_2 and $(U,Gd)O_2$. In: Proceedings of the ANS Topical Meeting on LWR Fuel Performance, April 10–13, 2000. Park City, UT.
63. Kinoshita, M., Sonoda, T., Kitajima, S. *et al*., 2004. High burnup rim project (III): Properties of rim-structured fuel. In: Proceedings of the 2004 ANS International Meeting on LWR Fuel Performance, p. 207. Orlando, FL.
64. Staicu, D., Rondinella, V.V., Walker, C.T., *et al*., 2014. J. Nucl. Mater 453 (1–3), 259–268.
65. Kinoshita, M., Sonoda, T., Kitajima, S. *et al*., 2000. High burnup rim project (II): Irradiation and examination to investigate rim-structured fuel. In: Proceedings of the ANS Topical Meeting on LWR Fuel Performance, April 9–13, 2000. Park City, UT.
66. Massih, A.R., Persson, S., Weiss, Z., 1992. J. Nucl. Mater. 188, 323–330.
67. Yagnik, S., Rashid, Y., Dunham, R., Montgomery, R., 2004. Fuel Analysis and Licensing Code: FALCON MOD01 Volume 1: Theoretical and Numerical Bases. CA: EPRI Palo Alto, p. 1011307.
68. De Bruycker, F., Boboridis, K., Poeml, P., Konings, R.J.M., Manara, D., 2011. J. Nucl. Mater. 416, 166.
69. Böhler, R., Welland, M.J., Prieur, D., *et al*., 2014. J. Nucl. Mater. 448 (1–3), 330–339.
70. Kato, M., Morimoto, K., Sugata, H., *et al*., 2008. J. Nucl. Mater. 373, 237–245.
71. Carbajo, J.J., Yoder, G.L., Popov, S.G., Ivanov, V.K., 2001. J. Nucl. Mater. 299, 181–198.
72. Hirosawa, T., Sato, I., 2011. J. Nucl. Mater. 418, 207–214.
73. Manara, D., Ronchi, C., Sheindlin, M., Lewis, M., Brykin, M., 2005. J. Nucl. Mater. 342, 148–163.
74. Kato, M., Morimoto, K., Sugata, H., *et al*., 2008. J. Alloy. Compd. 452 (1), 48–53.
75. Guéneau, C., Dupin, N., Sundman, B., *et al*., 2011. J. Nucl. Mater. 419, 145–167.
76. Konno, K., Hirosawa, T., 1998. J. Nucl. Sci. Technol. 35, 494.
77. Konno, K., Hirosawa, T., 2002. J. Nucl. Sci. Technol. 39 (7), 771–777.
78. Kang, K.W., Yang, J.H., Kim, J.H., *et al*., 2007. Thermochem. Acta 455, 134–137.
79. Beals, R.J., Handwerk, J.H., Wrona, B.J., 1969. J. Am. Ceram. Soc. 52, 578.
80. Yamanouchi, S., Tachibana, T., Tsukui, K., Oguma, M., 1988. J. Nucl. Sci. Technol. 25 (6), 528–533.